

ECLOGITE INDUCED DEFORMATION OF THE SIBERIAN CRATON

M.Sc. THESIS

Açelya BALLI

Department of Solid Earth Sciences

Geodynamics Programme

Thesis Advisor: Assoc. Prof. Oğuz GÖĞÜŞ

JUNE 2019

ECLOGITE INDUCED DEFORMATION OF THE SIBERIAN CRATON

M.Sc. THESIS

**Açelya BALLI
(602171001)**

Department of Solid Earth Sciences

Geodynamics Programme

Thesis Advisor: Assoc. Prof. Oğuz GÖĞÜŞ

JUNE 2019

İSTANBUL TEKNİK ÜNİVERSİTESİ ★ AVRASYA YER BİLİMLERİ ENSTİTÜSÜ

SİBİRYA KRATONUNUN EKLOJİT VARLIĞINDA DEFORMASYONU

YÜKSEK LİSANS TEZİ

Açelya BALLI

(602171001)

Katı Yer Bilimleri Anabilim Dalı

Jeodinamik Programı

Tez Danışmanı: Doç. Dr. Oğuz GÖĞÜŞ

HAZİRAN 2019

Açelya BALLI, a M.Sc. student of ITU Graduate School of Eurasia Institute of Earth Sciences student ID 602171001, successfully defended the thesis/dissertation entitled “ECLOGITE INDUCED DEFORMATION OF THE SIBERIAN CRATON”, which she prepared after fulfilling the requirements specified in the associated legislations, before the jury whose signatures are below.

Thesis Advisor: **Assoc Prof. Oğuz GÖĞÜŞ**
Istanbul Technical University

Jury Members: **Prof. Dr. Hans THYBO**
Istanbul Technical University

Dr. Ebru ŞENGÜL-ULUCAOK
Canakkale Onsekiz Mart University

Date of Submission : 3 May 2019
Date of Defense : 10 June 2019





To my brother,



FOREWORD

I would like to thank my thesis supervisor Assoc. Prof. Dr. Oğuz H. Göğüş for his continuous guidance, support and patience during my education. I am very grateful to have agreed to work with him as a master student.

I am beholden to Eurasia Institute of Earth Sciences for providing me an office at the university during my study.

I also would like thank to Prof. Dr. Irina Artemieva, Prof. Dr. Hans Thybo and Dr. Ebru Şengül Uluocak for their invaluable time and effort to improve my work. I am also very grateful to them for their crucial contributions to my master thesis.

I am very honored to work with master students, Uğurcan Çetiner, Ömer Bodur and Barış Şen.

I am indebted to my dear friends Ceyhun Erman, Hacı Ahmet Gezgin, Burcu Değerli, Caner Memiş.

Finally, I would like to thank my parents Yalçın Ballı and Şebnem Ballı for their unrequited love and support to me during my whole life.

June 2019

Açelya BALLI



TABLE OF CONTENTS

	<u>Page</u>
FOREWORD	ix
TABLE OF CONTENTS	xi
ABBREVIATIONS	xiii
SYMBOLS	xv
LIST OF TABLES	xvii
LIST OF FIGURES	xix
SUMMARY	xxi
ÖZET	xxiii
1. INTRODUCTION	1
1.1 Geologic Setting of Siberian Craton.....	3
1.2 Objectives.....	5
2. RESEARCH METHOD	7
3. EXPERIMENTAL RESULTS	11
3.1 Effect of Mantle Lithosphere Density	11
3.1.1 Localized (large scale convection).....	12
3.1.1.1 Experiment #A1 (reference model).....	12
3.1.1.2 Experiment #A2	12
3.1.1.3 Experiment #A3	14
3.1.2 Non-localized deformation.....	16
3.1.2.1 Experiment #B1	16
3.1.2.2 Experiment #B2	18
3.1.3 Pierce through.....	20
3.1.3.1 Experiment #C1	20
3.1.3.2 Experiment #C2	22
3.1.4 High degree deformation.....	24
3.1.4.1 Experiment #D1.....	24
3.2 Effect of Eclogite Size and Density.....	26
3.3 Model Results Against Observations	30
4. CONCLUSION	35
REFERENCES	37
CURRICULUM VITAE	41



ABBREVIATIONS

LAB : Lithosphere Asthenosphere Boundary

Ma : Million Years Ago

MOHO: Mohorovicic Discontinuity





SYMBOLS

κ	: Thermal conductivity
τ	: Shear stress
C	: Cohesion
σ	: Normal stress
g	: Gravity vector
t	: Time
u, v	: Displacement vector components
T	: Temperature
C_p	: Heat capacity
H	: Rate of internal heat production
α	: Thermal expansion coefficient
ρ	: Density
θ	: Angle of friction
$\dot{\epsilon}$: Strain rate
A	: Viscosity parameter
n	: Power exponent
Q	: Activation energy
R	: Ideal gas constant



LIST OF TABLES

	<u>Page</u>
Table 2.1 : The rheological parameters.	9
Table 3.1 : The physical parameters.....	11





LIST OF FIGURES

	<u>Page</u>
Figure 1.1 : Basements of the cratons (Lee et al., 2011). Cratons are labels as follows: 1. Slave, 2. Wyoming, 3. Superior, 4. Greenland, 5. Fennoscandian, 6. Siberian, 7. North China, 8. West Australian, 9. Indian, 10. Tarim, 11. Tanzanian, 12. South African, 13. Congo, 14. West African, 15. Amazonia, 16. Colorado Plateau.....	2
Figure 1.2 : Destruction mechanism of the lithosphere (Artemieva, 2011).	2
Figure 1.3 : Siberian craton with age and magmatic features modified after (Cherepanova et al., 2013, Cherepanova & Artemieva, 2015).....	4
Figure 1.4 : Free air gravity anomaly map of Siberian craton (Cherepanova et al., 2013).....	5
Figure 2.1 : Initial model setup.	8
Figure 3.1 : Mantle Lithosphere Mechanism Diagram	11
Figure 3.2 : Geodynamic evolution of the model setup #A1: eclogite block size 25 km x 100 km, eclogite block density 3500 kg/m ³ , density differences 60 kg/m ³	13
Figure 3.3 : MOHO vs. time (at x=1000 km).	14
Figure 3.4 : Geodynamic evolution of the model setup #A2: eclogite block size 10 km x 250 km, eclogite block density 3600 kg/m ³ , density differences 40 kg/m ³	15
Figure 3.5 : MOHO depth vs. time (at x=1000 km).....	16
Figure 3.6 : Geodynamic evolution of the model setup #A3: eclogite block size 5 km x 500 km, eclogite block density 3500 kg/m ³ , density differences 60 kg/m ³	17
Figure 3.7 : MOHO vs. time (at x=1000).	18
Figure 3.8 : Geodynamic evolution of the model setup #B1: eclogite block size 5 km x 500 km, eclogite block density 3700 kg/m ³ , density differences 20 kg/m ³	19
Figure 3.9 : MOHO vs. time (at x=1000 km).	20
Figure 3.10 : Geodynamic evolution of the model setup #B2: eclogite block size 5 km x 500 km, eclogite block density 3600 kg/m ³ , density differences 20 kg/m ³	21
Figure 3.11 : MOHO vs. time (at x=1000 km).	22
Figure 3.12 : Geodynamic evolution of the model setup #C1: eclogite block size 25 km x 100 km, eclogite block density 3600 kg/m ³ , density differences 40 kg/m ³	23
Figure 3.13 : MOHO vs time (at x=1000 km).	24
Figure 3.14 : Geodynamic evolution of the model setup #C2: eclogite block size 25 km x 100 km, eclogite block density 3600 kg/m ³ , density differences 60 kg/m ³	25
Figure 3.15 : MOHO vs. time (at x=1000 km).	26

Figure 3.16 : Geodynamic evolution of the model setup #D1: eclogite block size 10 km x 250 km, eclogite block density 3600 kg/m ³ , density differences 0 kg/m ³	27
Figure 3.17 : MOHO vs. time (at x=1000 km).....	28
Figure 3.18 : Deformational behavior diagram.	29
Figure 3.19 : Change in MOHO thicknesses with varying eclogite densities for 5 km x 500 km eclogite blocks.....	31
Figure 3.20 : Change in MOHO thicknesses with varying eclogite densities for 10 km x 250 km eclogite blocks.....	31
Figure 3.21 : Change in MOHO thicknesses with varying eclogite densities for 25 km x 100 km eclogite blocks.....	31
Figure 3.22 : Change in LAB thicknesses with varying eclogite densities for 5 km x 500 km eclogite blocks.	32
Figure 3.23 : Change in LAB thicknesses with varying eclogite densities for 10 km x 250 km eclogite blocks.	32
Figure 3.24 : Change in LAB thicknesses with varying eclogite densities for 25 km x 100 km eclogite blocks.	32
Figure 3.25 : MOHO and LAB depths (modified after Cherepanova & Artemieva, 2015).....	33
Figure 3.26 : MOHO and LAB depth vs. horizontal distance (Cross sections taken from MOHO and LAB maps).....	33
Figure 3.27 : MOHO and LAB depth comparison of real data with model results..	34

ECLOGITE INDUCED DEFORMATION OF THE SIBERIAN CRATON

SUMMARY

The deformation of the cratons, whose roots are approximately 250 km deep is very difficult. The removal of the mantle lithosphere, which is one of the proposed mechanisms for the deformation of the craton that is stable for long periods, is carried out by many different processes. Deformation of the craton as a result of a gravitational instability is one of the most likely mechanisms. According to isopycnic hypothesis, lithospheric mantle of cratons thought to be buoyant due to their depleted composition, even though most of them Archean in age and cold. Since the mantle lithosphere of the craton is lighter in density than asthenosphere, an additional force is required for a gravitational instability to occur. This thermo - mechanical force causes deformation of the roots of the craton by creating an instability between the mantle lithosphere and the asthenosphere.

The Siberian craton is one of the world's largest Archean - Proterozoic cratons. The Siberian craton has approximately 100 - 1300 m surface topography, 35 - 53 km MOHO thickness, and a maximum depth of 350 km LAB which are acquired from petrological studies, seismic tomography and gravity anomalies. Specifically, the LAB varies among 170-350 km and such depth change is not well understood. Until the formation of the Siberian craton is completed, it hosts many tectonic and magmatic events. These include active margin zones, continent collisions, and rift zones. As a result of pressure change in the active boundary regions, the transformation of basalt to eclogite takes place. Therefore, it creates a gravitational instability in the environment. Gravity anomalies observed near kimberlite fields, reflect the possibility of denser eclogitic bodies under the crust of Siberian craton. Our study focuses on testing potential deformation of the Siberian continental lithosphere with the presence of these eclogitic bodies. We performed 2D numerical experiments to investigate the effects of eclogite blocks that are varying in size and density. Crust rheology was prepared in accordance with Siberian craton. The density of the mantle lithosphere ($3330 \text{ kg / m}^3 - 3410 \text{ kg / m}^3 + 20 \text{ kg / m}^3$) is changed to observe its effect on the system, and eclogite blocks of different size (5 km x 500 km, 10 km x 250 km, 25 km x 100 km) are added to the lower crust base to start a gravitational instability.

According to model results, depending on the deformation of the mantle lithosphere, eclogite block can either stay attached to the lower crust, or it can be detached from it. In the case where the eclogite block attached to the lower crust, two different conditions: localized deformation (do not occur the drip mechanism) and non-localized deformation occurs due to the small-scale convection movement. Also, two different removal mechanism for the case where eclogite becomes detached are also observed: high degree deformation of mantle lithosphere, and the eclogite block pierce through the mantle lithosphere. Comparison of experimental results with geophysical data for MOHO and LAB depths showed that, the most convenient models for Siberian craton

are the models where the dripping were not observed. Mantle lithosphere densities of 3350 kg / m^3 or less yields the most consistent results. While the width of the eclogite block causes high-degree deformation, it is observed that with increasing thickness it leads to formation of viscous drips. Taking MOHO and LAB depths into account obtained from the model results, it has been observed that the model #A1, #A2 and #A3 agrees well with the BB' cross-section at 20.92 Ma, 25.36 Ma and 20.92 Ma, respectively. Experimental results indicate that, eclogite block(s) under the Siberian craton may still be there and craton itself does not undergo any significant deformation.



EKLOJİT VARLIĞINDA SİBİRYA KRATONUN DEFORMASYONU

ÖZET

Kratonlar kalın litosferik köklere, düşük ısı akısına sahip olan yapılardır. Birçoğu Arkeen yaşlı olduğu için yoğunluklarının fazla olduğu düşünülse de litosferik mantoları nötral olarak yüzebilirlikleri fazladır. Kratonik alanlardaki aktif sınır bölgesi, birikim ya da tektonik kalınlaşma prosesleri kraton altı manto litosferinin tabanında kalın termal sınır bölgesinin oluşmasına neden olmaktadır. Derinlik ile artan sıcaklık, nötral olarak yüzebilen manto peridotunu tükenmiş hale getirerek, daha duraylı olmasına yol açmaktadır. Bu süreç boyunca biriken kalıntı, kratonik manto litosferi altında birikerek kalın, yüzebilirliği fazla olan termal sınır katmanının oluşmasını sağlamaktadır. Böylece termal sınır katmanı konvektif dengesizliklere karşı daha dayanıklı hale gelmektedir. Kökleri yaklaşık olarak 250 km derine inen kratonların deformasyonu bu nedenle oldukça zordur. Uzun dönemler boyunca stabil olan kratonların deformasyonu için önerilen mekanizmalardan biri olan manto litosferinin taşınması, farklı şekillerde gerçekleşmektedir. Bunlar arasında bulunan gravitasyonel bir dengesizlik sonucu kratonun deformasyonu, en olası mekanizmalardan biridir. Kratonların, manto litosferi, astenosfere oranla daha düşük yoğunlukta olduğundan gravitasyonel bir dengesizliğin gerçekleşebilmesi için dışarıdan bir kuvvet gerekmektedir. Bu termo – mekanik kuvvet manto litosferi ile astenosfer arasında bir dengesizlik yaratarak kratonun köklerinin deformasyonuna neden olmaktadır.

Sibirya kratonu Dünya'nın en büyük Arkeen – Proterozoik yaşlı kratonudur. Sibirya kratonu elde edilen sismik hızlar doğrultusunda yaklaşık olarak 100 – 1300 m yüzey topografyasına, 35 – 53 km MOHO kalınlığına, maximum 350 km LAB derinliğine sahiptir. Sibirya kratonunun oluşumu tamamlanana kadar olan süreçte birçok tektonik ve magmatik olaya ev sahipliği yapmıştır. Bunlar arasında aktif sınır bölgeleri, kıta çarpışmaları ve rift bölgelerinin oluşması gibi tektonik süreçler bulunmaktadır. Aktif sınır bölgelerinde görülen basınç değişimi sonucu bazaltın eklojite dönüşümü gerçekleşmektedir. Eklojit kayası çevresini saran kütlelerden daha yoğun olan bir kayadır. Bu nedenle bulunduğu ortamda gravitasyonel bir dengesizlik yaratmaktadır.

Bu çalışma için 2 boyutlu numerik modeller tercih edilmiştir. Kabuk reolojisi iki kısma ayrılarak, üst katman için kuru kuvarsit (20 km) ve alt katman için felsik granülit (15 km) tercih edilmiştir. Manto litosferi 200 km kalınlığında olup, manto litosferinin yoğunluk ($3330 \text{ kg/m}^3 - 3410 \text{ kg/m}^3 + 20 \text{ kg/m}^3$) aralığı değiştirilerek, sisteme etkisinin nasıl olduğuna bakılmaktadır. Eklojit varlığında gerçekleşecek olan deformasyona bakıldığı için farklı yoğunlukta ($3400 \text{ kg/m}^3 - 3700 \text{ kg/m}^3 + 100 \text{ kg/m}^3$) ve farklı boyutta eklojit blokları (5 km x 500 km, 10 km x 250 km, 25 km x 100 km) alt kabuk tabanına eklenerek gravitasyonel bir dengesizliğin başlaması sağlanmaktadır. Model parametreleri Sibirya kratonu üzerinde gerçekleştirilen petrolojik çalışmalar baz alınarak düzenlenmiştir.

Model sonuçları eklojit bloğunun hareketine bağlı olarak, eklojitin alt kabuğa bağlı kaldığı ve alt kabuktan koptuğu mekanizma olarak ikiye ayrılmaktadır. Eklojit bloğunun alt kabuktan kopmadığı durumda damlama mekanizmasının gerçekleşmediği (lokalize deformasyon) ve küçük ölçekli konveksiyon hareketine bağlı oluşan deformasyon (lokalize olmayan deformasyon) gözlenirken, alt kabuktan koptuğu durumlarda manto litosferinin yüksek dereceli deformasyonu ve eklojit bloğunun manto litosferini delip geçtiği farklı mekanizmalar tespit edilmiştir. Lokalize deformasyon viskoz damlama mekanizmasının gerçekleşmediği fakat manto litosferinin konveksiyon hareketi sonucunda lokal olarak deformasyon gerçekleşen durum olarak nitelendirilmiştir. Bu model davranışının gerçekleşmesi için genellikle manto litosferi ve astenosfer arasındaki yoğunluk farkının 40 kg/m^3 'e eşit ya da daha büyük ve manto litosfer yoğunluklarının 3330 kg/m^3 ya da 3350 kg/m^3 olması gerekmektedir. Lokalize olmayan deformasyon davranışında eklojit bloğu alt kabuktan kopacak kadar güçlü değildir. Bu nedenle, astenosferin yarattığı küçük çaplı konveksiyon kuvvetleri manto litosferinin parçalanmasına ve deformasyonuna sebep olmaktadır. Bu davranışın gerçekleşebilmesi için astenosfer ve manto litosferi arasındaki yoğunluk farkının 20 kg/m^3 'e eşit ya da daha az olması gerekmektedir. Eklojit bloğunun alt kabuktan ayrılıp, manto litosferini delip geçtiği model sonuçları, yalnızca $25 \text{ km} \times 100 \text{ km}$ eklojit boyutunda gerçekleştiği gözlenmektedir. Eklojit bloğunun manto litosferini delip geçebilmesi için, boyut koşulunun yanı sıra, yoğunluğunun da 3600 kg/m^3 ' ten daha fazla olması gerekmektedir. Yüksek dereceli deformasyonun gerçekleştiği davranışta ilk süreçte eklojit bloğu duraysız hale gelip, manto litosferinin tabanında birçok dengesizliğin olmasına neden olmaktadır. Eklojit bloğunun aşağı doğru hareketi beraberinde manto litosferini de getirerek, astenosfer içine batmasına neden olmaktadır. Bu model davranışında en önemli parametre eklojit bloğunun boyutu olmaktadır. Eklojit bloğunun kalınlığının artması ile manto litosferinin yüksek dereceli deformasyonu gerçekleşirken, azalması ile lokalize olmayan davranış gerçekleşmektedir. İkincil önemli parametre ise manto litosferi ve astenosfer arasındaki yoğunluk farkının azalmasıdır. Bazı yüksek dereceli deformasyon deney sonuçlarında manto litosferi çok fazla duraysız hale gelerek tamamen astenosfer içine damladığı ve kabuğun astenosfer ile temas ettiği gözlenmiştir.

Model sonuçları doğrultusunda eklojit bloğunun kalınlığının ve uzunluğunun aynı zamanda yoğunluğunun sisteme farklı etkileri olduğu gözlenmektedir. Eklojit bloğu ve manto litosferi yoğunluklarına göre yapılan sınıflandırmada her eklojit boyutu için farklı sistematik gözlenmiştir. $25 \text{ km} \times 100 \text{ km}$ eklojit bloğu için eklojitin manto litosferini delip geçtiği, lokalize ve baskın olarak yüksek dereceli deformasyon davranışları oluşturmaktadır. $10 \text{ km} \times 250 \text{ km}$ eklojit boyutlarında lokalize ve lokalize olmayan deformasyon hakim iken, yüksek dereceli deformasyon eklojitin kalınlığının azalmasına bağlı olarak daha az gözlenmektedir. En küçük kalınlığa sahip olan $5 \text{ km} \times 500 \text{ km}$ eklojit bloğu lokalize ve lokalize olmayan davranış sergilemektedir.

Model sonuçları Sibiry kratonunun MOHO ve LAB derinliği ile kıyaslanmış ve en uygun verilerin lokalize deformasyon mekanizmasının gerçekleştiği modellerde tespit edilmiştir. MOHO ve LAB derinlik haritalarından alınan dört farklı kesit arasından BB' kesitinin, seçilen model setleri ile en uyumlu derinlik sonuçlarını verdiği gözlenmiştir. Ayrıca, manto litosfer yoğunluğu için 3350 kg/m^3 ve daha az olan yoğunlukların en uyumlu sonuçları verdiği görülmektedir.

Eklojit bloğunun genişliği yüksek dereceli deformasyona neden olurken, kalınlığının damlama mekanizmasına neden olduğu gözlenmektedir. Model verileri neticesinde

Sibirya kratonu altında var olan eklojit bloğunun hala orada olabileceği ve önemli bir deformasyon geçirmediği düşünülmektedir.





1. INTRODUCTION

The most distinctive features of the cratons, except for the thick lithospheric roots (>250 km), are the low heat flow (45mW/m^2) and their buoyant and rigid lithospheric mantles (Jordan, 1978; Kelly et al., 2003; Artemieva, 2011; Zhu et al., 2012). Commonly, older rocks have higher densities. Even though, most of the cratons are Archean in age (Figure 1.1), their lithospheric mantles are thought to be neutrally buoyant. It has been suggested that, their highly depleted sub-continental lithospheric mantles with high Mg content is the main reason for this buoyancy. Jordan (1988) calculated that, an increase of one unit in the Mg#, corresponds to a density increase caused by a temperature decrease of $200\text{ }^\circ\text{C}$. Hence, positive buoyancy of the depleted lithospheric mantle can compensate the difference caused by conductive cooling, and it can lead craton to become neutrally buoyant (Herzberg & Rudnick, 2012, Artemieva et al., 2019).

Subduction, accumulation, or any tectonic thickening process in the cratonic areas causes the formation of a thick thermal boundary layer at the base of the sub-cratonic mantle lithosphere. On greater depths with increasing temperatures, neutrally buoyant mantle peridotites become depleted and becomes more stable. During this process, the stratified residues accumulate under the cratonic mantle lithosphere and form thick, buoyant thermal boundary layer. Thus, the thermal boundary layer becomes more resistant to convective instabilities (Kelemen et al., 1998).

With their thick lithospheric roots and passive tectonism (since Precambrian), the cratons are considered to be the most stable formations in the world (Liao et al., 2017). Although they are the most stable areas, some of them have been subjected to deformation due to magmatic and tectonic events. The mantle lithosphere of many cratons, such as Northern China, Siberia and Wyoming, have undergone deformation (Artemieva, 2011, Zhu et al., 2012). Many different mechanisms (Figure 1.2) like convective removal, basal traction, subduction, rheological weakening and thermo-magmatic erosion are proposed for the deformation of the cratons, that form the core of the continents (Lee et al., 2011).

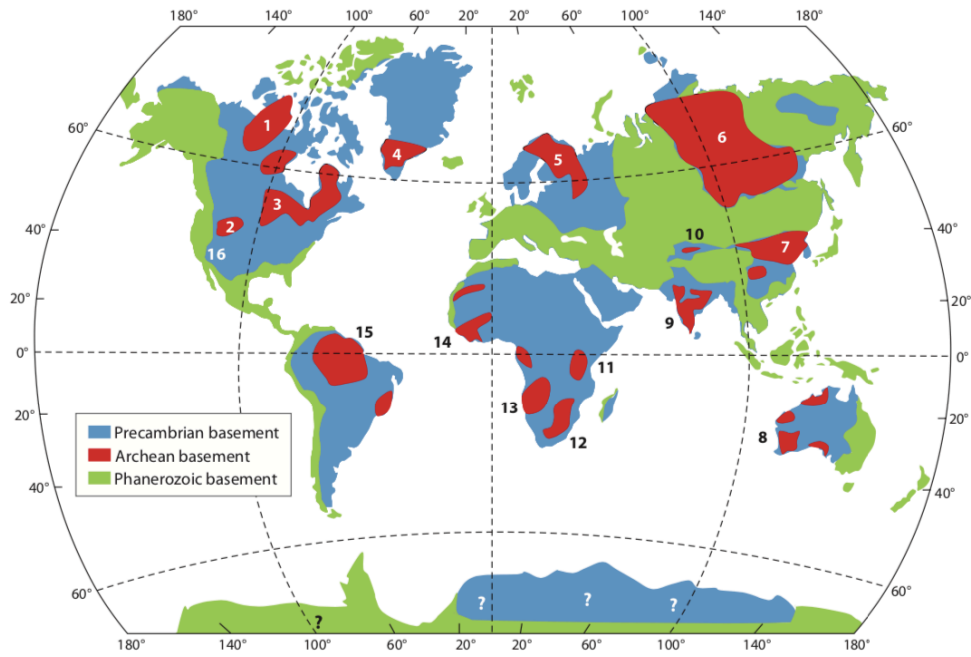


Figure 1.1 : Basements of the cratons (Lee et al., 2011). Cratons are labels as follows: 1. Slave, 2. Wyoming, 3. Superior, 4. Greenland, 5. Fennoscandian, 6. Siberian, 7. North China, 8. West Australian, 9. Indian, 10. Tarim, 11. Tanzanian, 12. South African, 13. Congo, 14. West African, 15. Amazonia, 16. Colorado Plateau.

The convective removal mechanism results from density (or temperature) difference between two fluids. The density varies depending on the temperature, causing a gravitational instability between the two melts. This instability leads to deformation of the continental lithosphere. Weak zones on the crust, perturbation located on mantle lithosphere, crustal thickening as a result of the continental collision, chemical alteration of the mantle lithosphere and a heavy mineral remaining in the lower crust, such as eclogite, might cause a gravitational instability to grow (Pysklywec & Cruden, 2004).

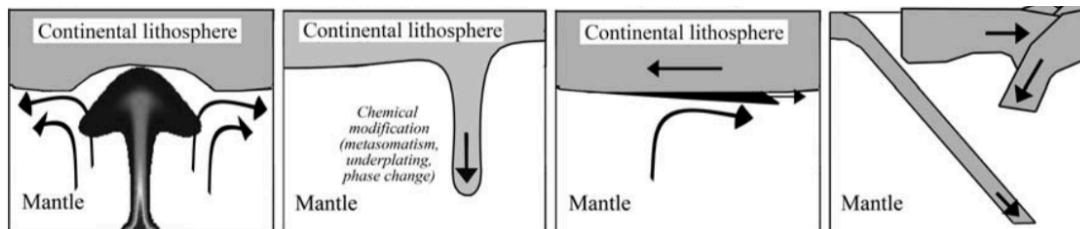


Figure 1.2 : Destruction mechanism of the lithosphere (Artemieva, 2011).

Eclogite is coarse – grained metamorphic rock which can be formed under high pressure and temperature (Anderson, 2008).

It can occur as a result of metamorphism of mafic crustal rock in subduction zones and may form due to crustal thickening in continent – continent collision zones (Kopylova et al., 2016). Thus, eclogite can be formed at a depth of 40 km to 150 km.

The Siberian craton, one of the largest and oldest cratons in the world, has undergone many tectonism and volcanism prior to its formation. Presence of denser rocks located in the lower crust can be resulted from these tectonic and volcanic events (Snyder et al., 1997). This study, focuses on the deformation which may arise from these denser (eclogitic) rocks. Gravity anomalies observed near kimberlite fields, reflect the possibility of denser eclogitic bodies under the crust of Siberian craton. Our study focuses on testing potential deformation of the Siberian continental lithosphere with the presence of these eclogitic bodies.

1.1 Geologic Setting of Siberian Craton

The Siberian craton was formed by the joining of many Archean and Proterozoic terranes (Rosen et al., 1994). The Siberian Craton is surrounded by the Anabar shield in the southeast, the Yenisey belt extending from the southeast to the west, the Tunguska basin in the northwest and the Aldan shield in the northeast (Figure 1.3).

Approximately 2 billion years ago, Anabar and Aldan blocks began to form as a result of a collision, and the two blocks separated from each other with Akitkan magmatic belt, which is formed during that time (Cherepanova & Artemieva, 2015). The majority of the craton is covered with Riphean – Phanerozoic aged sediments, while the other part is covered with Permo – Triassic flood basalts due to large igneous provinces at the northwest (Rosen et al., 2008).

During the Proterozoic period, a rift system on southern part of Siberian craton began to form, and until the Carboniferous time it had been home to many other rifting and collapsing events (Cherepanova et al., 2013).

The magmatic units of the Siberian craton consist of:

1. Neoproterozoic aged mafic dike volcanism in south – southeast part,
2. Phanerozoic aged kimberlite volcanism in northeastern part,
3. Permo – Triassic aged trap basalt volcanism in northwest part.

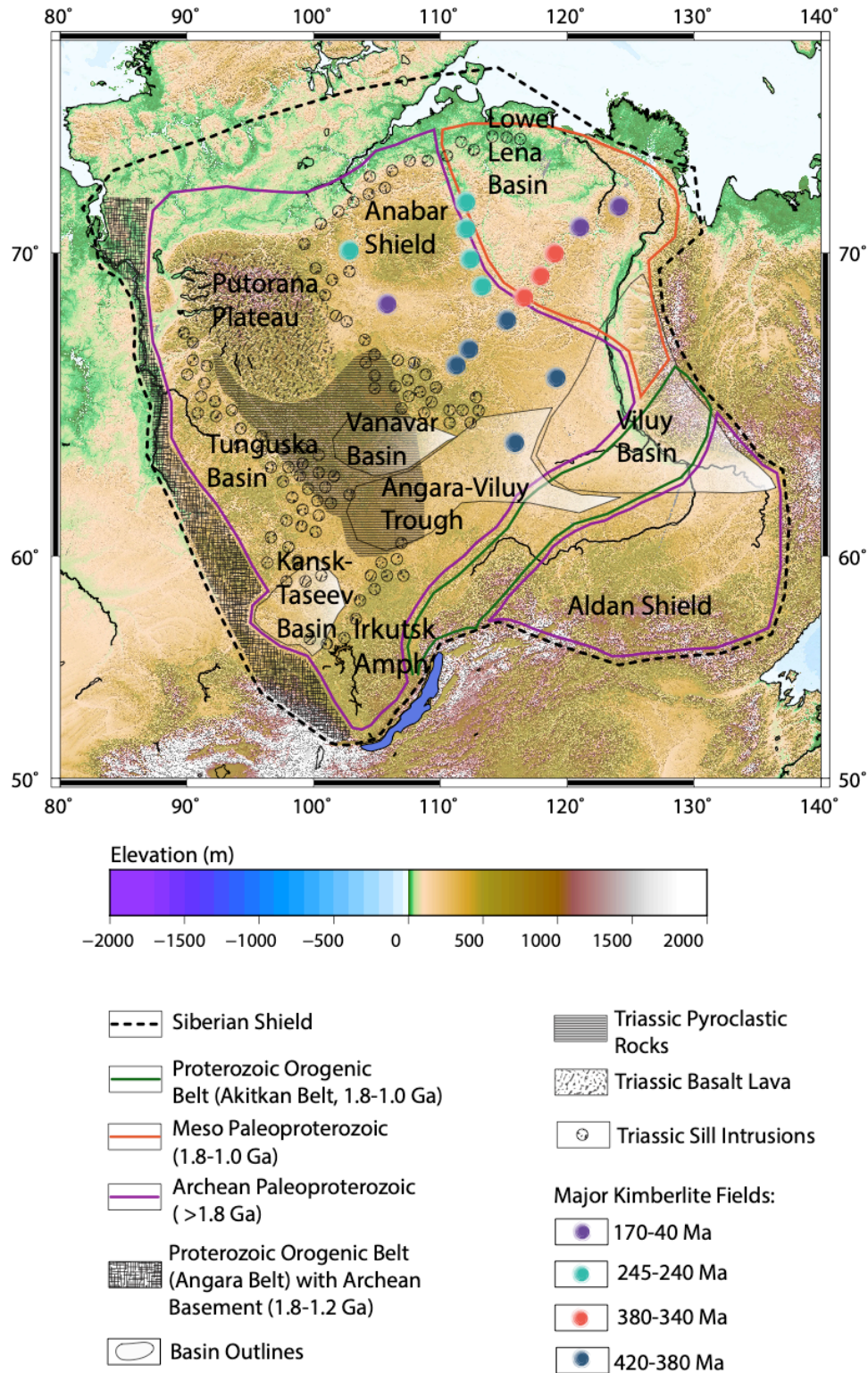


Figure 1.3 : Siberian craton with age and magmatic features modified after (Cherepanova et al., 2013, Cherepanova & Artemieva, 2015).

The surface topography of the Siberian craton varies between 100 – 1300 m. It is thought that most of the topographic features of the region had been erased due to erosion (Cherepanova et al., 2013).

Since the crustal rocks of the craton have a heterogeneous structure, it has a rheology that is predominantly of granite – greenstone and granulite - gneiss, although it varies from place to place (Gladkochub et al., 2010). Seismic measurements showed that, the depth of the MOHO varies between 35 – 54 km. The Lithosphere – Asthenosphere Boundary (LAB) thicknesses varies from 100 km to 350 km (Cherepanova et al., 2013). Lithospheric mantle thickness of the central Siberian craton, are measured to be 300 ± 30 km thick. Petrological studies, that have been carried out with mantle-derived xenoliths from kimberlite pipes are indicative of a highly depleted mantle (Kuskov et al., 2014).

As a result of petrological studies conducted with the samples that have been taken from kimberlite pipes, it was determined that heavy minerals, especially eclogite, were located within the region (Snyder et al., 1997). Cherepanova & Artemieva, (2015) stated that heavy minerals have been identified different parts of the region especially northern and southern parts (Figure 1.4).

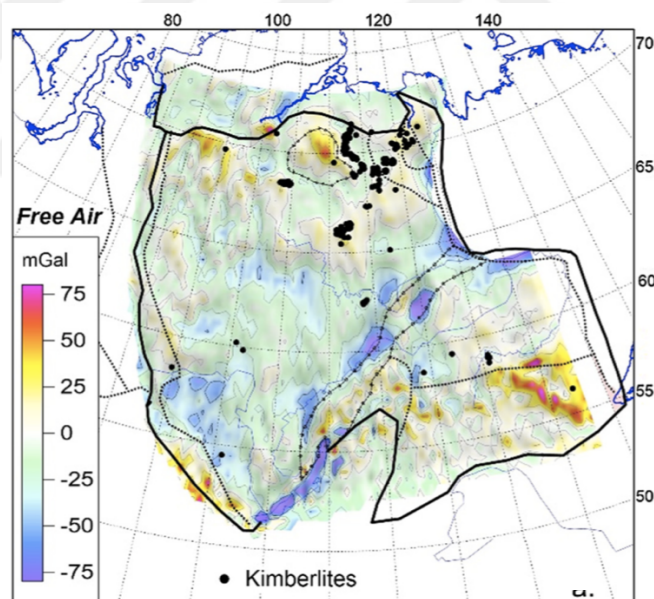


Figure 1.4 : Free air gravity anomaly map of Siberian craton (Cherepanova et al., 2013).

1.2 Objectives

There are several hypothetical geodynamic models that attempt to explain the deformation of a cratonic mantle lithosphere (Artemieva & Mooney, 2004; Lee et al., 2011).

This study focuses on the viability of drip induced deformation of the cratonic roots, and classifying the different types of deformations with an extensive parameterization.

Main goals of the study are:

1. Understanding the impact of thickness and wideness of eclogitic bodies in such settings with numerical experiments,
2. Investigating effects of presence of the denser rocks found in areas with density anomalies; by comparing MOHO, LAB thicknesses, and temperature profiles to the model results.



2. RESEARCH METHOD

SOPALE is a 2D visco – plastic code that calculates the thermo – mechanical behavior of each layer with time. Eulerian grids calculate the pressure and velocity of the material using the Stokes equation, while Lagrangian grids responsible for measuring how much the edges of the grid deformed; and the computation of temperature, pressure and accumulated material (Fullsack, 1995).

Governing equations for momentum (Eq. 2.1), mass (Eq. 2.2) and internal energy (Eq.2.3) are given respectively,

$$\nabla(\sigma_{ij}) + \rho g = 0, \quad (2.1)$$

$$\nabla \cdot u = 0, \quad (2.2)$$

$$\rho C_p \left(\frac{\partial T}{\partial t} + u \cdot \nabla T \right) = \kappa \nabla^2 + \rho H, \quad (2.3)$$

where; u is fluid velocity, σ_{ij} is deviatoric stress tensor, T is temperature (K), C_p is heat capacity at constant pressure ($J \text{ kg}^{-1} \text{ K}^{-1}$) and H is the rate of internal heat production per unit mass ($W \text{ kg}^{-1}$). The parameters κ , ρ , α and g are the thermal conductivity ($m^2 \cdot s^{-1}$), density (kg/m^3), thermal expansion coefficient ($1/K$), and gravity vector ($m \cdot s^{-1}$), respectively.

Plastic deformation is calculated by,

$$\tau = C + \sigma \tan \theta \quad (2.4)$$

Where τ is shear stress (force per unit area), c is cohesion (Pa), σ is normal stress (Pa), θ is angle of friction. Viscous deformation is calculated through viscous flow law,

$$\dot{\epsilon} = A \sigma^n \exp\left(\frac{-Q}{RT}\right) \quad (2.5)$$

where $\dot{\epsilon}$ is represent strain rate (s^{-1}), A is viscosity parameter ($Pa^{-n} \cdot s^{-1}$), n is power exponent, Q activation energy ($kJ \cdot mol^{-1}$), R is the ideal gas constant ($J \cdot mol^{-1} \cdot K^{-1}$).

Density varies with changing temperature according to,

$$\rho(T) = \rho_0(1 - \alpha(T - T_0)), \quad (2.6)$$

Where ρ is density (kg/m^3) and T is temperature (K).

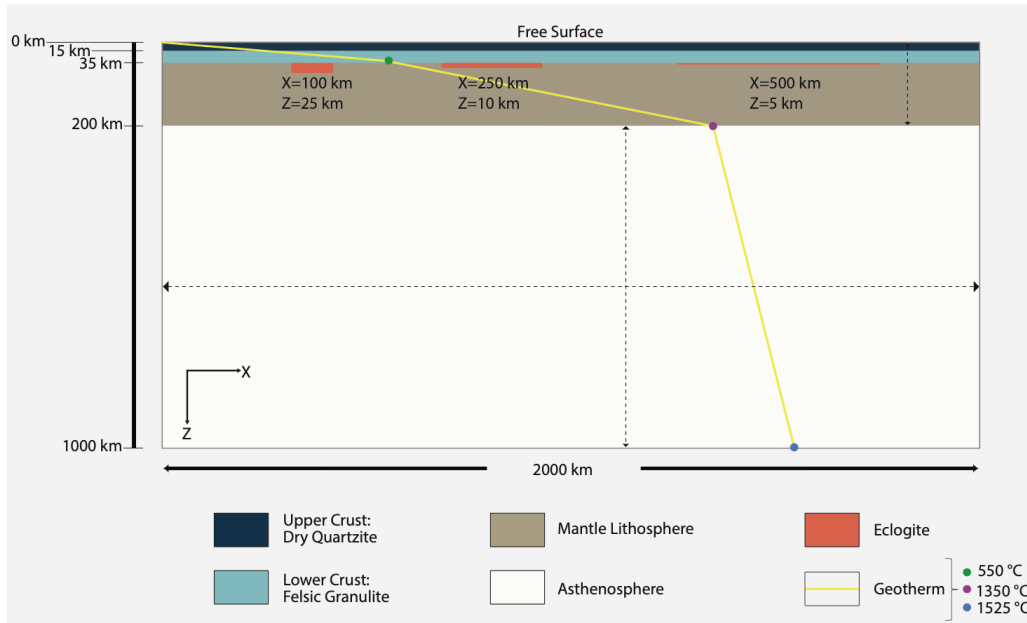


Figure 2.1 : Initial model setup.

Model domain is 2000 km width for x-axis and 1000 km thick for y-axis. The rheologies we used for upper crust (15 km) and lower crust (20 km) are dry quartzite and felsic granulite, respectively (Table 2.1). Plastic rheology chosen for the upper crust and viscous behavior for lower crust. We put different size of eclogitic bodies, which are 5 km x 500 km, 10 km x 250 km and 25 km x 100 km, under the lower crust to initiate the gravitational instability. The density of eclogite bodies varies between 3500 kg/m^3 and 3700 kg/m^3 with increments of 100 kg/m^3 . The selected density values are minimum and maximum eclogite densities in taken from literature (Hacker, 1996). Density of the mantle lithosphere increased from 3330 kg/m^3 to 3410 kg/m^3 by increments of 20 kg/m^3 . We used two different mantle lithosphere thicknesses, 200 km and 260 km, to measure the effect of thickness of the mantle lithosphere. The asthenosphere density ($\rho_{\text{ast.}}=3390 \text{ kg/m}^3$) is temperature dependent. In order to make experiments more suitable for cratonic environments, mantle lithosphere densities have chosen to be lower than the asthenosphere density for some experiments.

For some of them, higher densities (3390 kg/m^3 and 3410 kg/m^3) were chosen to observe the behavior of the mantle lithosphere and to test the parameter sweep. Surface temperature is $25 \text{ }^\circ\text{C}$, base of the crust is $550 \text{ }^\circ\text{C}$, base of the lithosphere is $1350 \text{ }^\circ\text{C}$ and

bottom boundary of the box is 1798 °C. For the top and the bottom boundary, free surface boundary conditions have been used to minimize the numerical topographic errors.

Table 2.1 : The rheological parameters.

Reference	Layers	Starting material	A (MPa ⁻ⁿ s ⁻¹)	n	Q (kJmol ⁻¹)
(Gleason & Tullis, 1995)	Upper Crust	Black Hills quartzite	$1.1 \times 10^{(-4 \pm 2)}$	4.0 ± 0.9	223 ± 56
(Ranalli, 2008)	Lower Crust	Felsic granulite	8.0×10^{-3}	3.1	243 ± 50
(Jin et al., 2001)	Eclogite	-	1.0×10^{-4}	3.4	480 ± 30
(Hirth & Kohlstedt, 1996)	Mantle Lithosphere	Wet olivine	4.89×10^6	3.5	515
(Hirth & Kohlstedt, 1996)	Asthenosphere	Wet olivine	4.89×10^6	3.5	515



3. EXPERIMENTAL RESULTS

3.1 Effect of Mantle Lithosphere Density

Depending on the behavior of the lithospheric mantle, we have divided the model results into 2 different behaviors which are (i) eclogite attached, (ii) eclogite detached (Figure 3.1). There are two distinct behavior for eclogite attached mechanism localized mantle lithosphere and non-localized mantle lithosphere. Pierce through and high degree deformation are the other behaviors for the eclogite detached behavior. The chosen models are presented in Table 3.1.

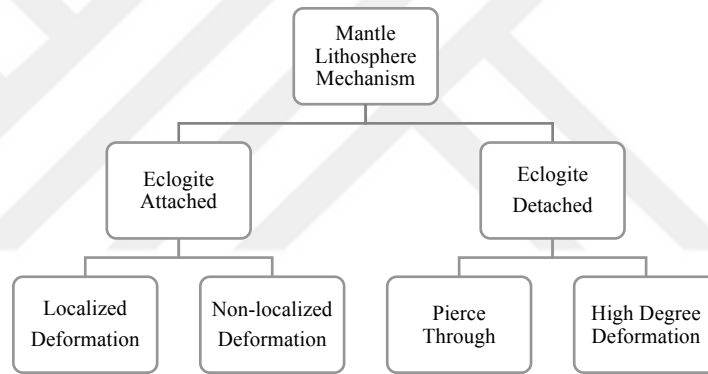


Figure 3.1 : Mantle lithosphere mechanism diagram.

Table 3.1 : The physical parameters for each model (*A1: Reference Model).

Experiment Name	Mantle Lithosphere Density (kg/m ³)	Eclogite Density (kg/m ³)	Eclogite Sizes (km x km)	Mechanism Behavior
*A1	3330	3500	25 x 100	Localized Deformation
A2	3350	3600	10 x 250	Localized Deformation
A3	3300	3500	5 x 500	Localized Deformation
B1	3370	3700	5 x 500	Non-localized Deformation
B2	3370	3600	5 x 500	Non-localized Deformation
C1	3350	3600	25 x 100	Pierce Through
C2	3330	3600	25 x 100	Pierce Through
D1	3390	3600	10 x 250	High Degree Deformation

3.1.1 Localized (large scale convection)

Models without distinct viscous dripping have been labeled as “localized deformation”. This behavior is observed when the density difference between the mantle lithosphere and asthenosphere is equal to or greater than 40 kg/m^3 ($\rho_{asth} - \rho_{mlith} = \Delta\rho = 40 \text{ kg/m}^3$). This behavior is only observed when the mantle lithosphere density is 3330 or 3350 kg/m^3 but it also depends on eclogite density and eclogite size that has been used in the models as well.

3.1.1.1 Experiment #A1 (reference model)

In this model 25 km thick and 100 km wide eclogite body, with a density of 3500 kg/m^3 , has imposed into the setup. Mantle lithosphere is 200 km thick and has a density of 3330 kg/m^3 . Density difference between the mantle lithosphere and the asthenosphere is 60 kg/m^3 .

Denser eclogitic body starts a downward movement, because it is denser than the surrounding rocks (Figure 3.2). Accordingly, it pulls down the rheologically weak lower crust with it. Consequently, a depression on the surface has been observed at $t=10.14 \text{ Ma}$. The instability of the mantle lithosphere that took place after 10 Ma, the LAB shows a depth of about 320 km. At 15.75 Ma, the surface topography starts to move upwards to reach isostatic equilibrium because of the thickened lower crust. This process goes on until the last time step, as eclogite continues to pull down the weak lower crust. After 30.75 Ma, the surface topography reaches about 1.3 km and the MOHO depth is 53 km. It has been observed that MOHO depth increased from 35 km to 53 km in $\sim 30 \text{ Ma}$ (Figure 3.3). Lithosphere – Asthenosphere boundary (LAB) undulates from 175 km on the thinnest parts to 320 km on the thickest parts. Model running time (30.75 Ma) was not long enough for eclogite to become separated from the lower crust, yet, it still led to formation of gravitational instability, caused MOHO to deepen and the mantle lithosphere to become unstable. In the last time period, LAB undulations are observed due to the gravitational instability created by eclogite.

3.1.1.2 Experiment #A2

In this model 10 km thick and 250 km wide eclogite body, with a density of 3600 kg/m^3 , has imposed into the setup. Mantle lithosphere is 200 km thick and has a density of 3350 kg/m^3 . Density difference between the mantle lithosphere and the

asthenosphere is 40 kg/m^3 . In this experiment (Figure 3.4), the density of the eclogite block is more than the density of the mantle lithosphere, therefore, negatively buoyant forces are acting on the mantle lithosphere.

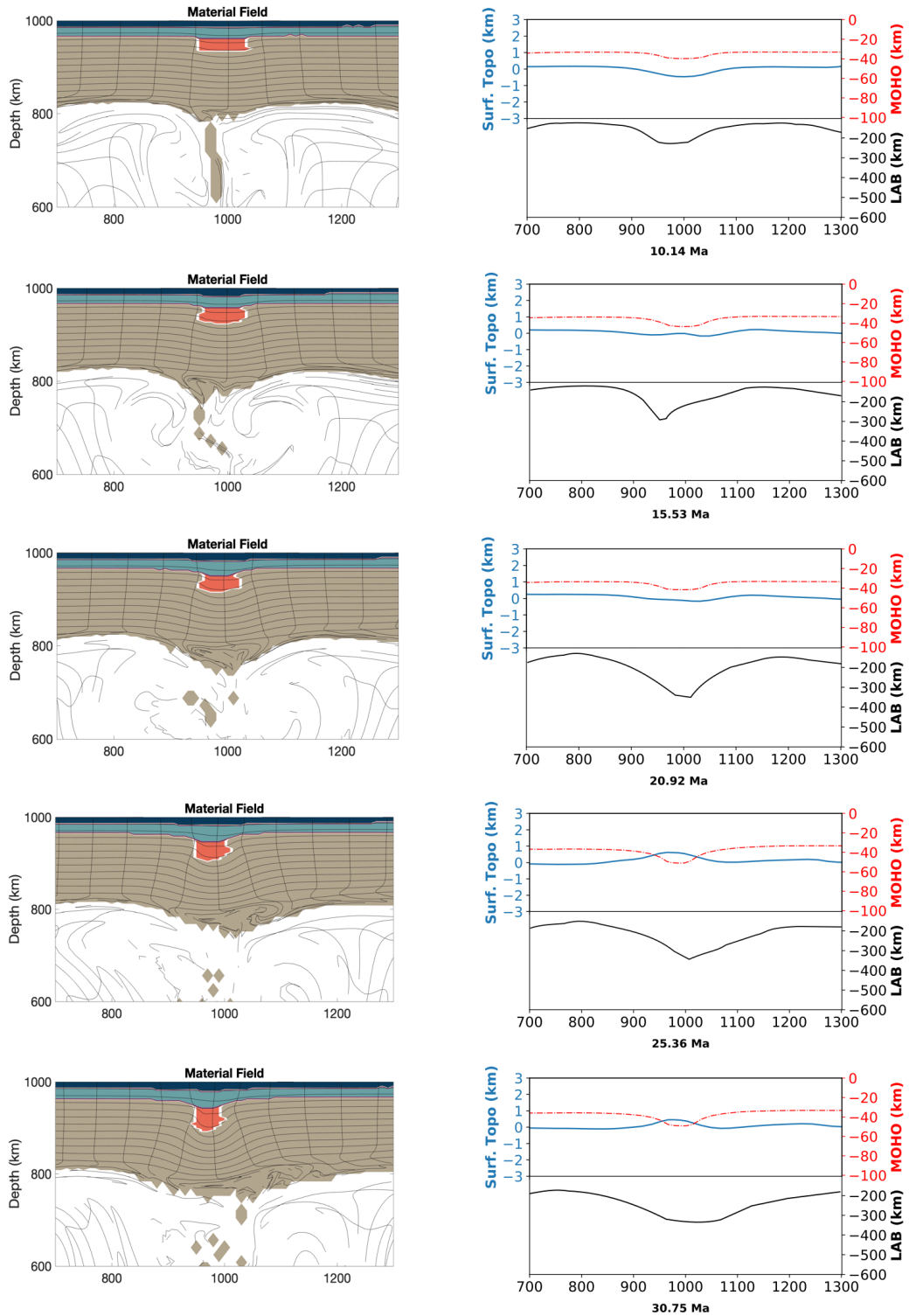


Figure 3.2 : Geodynamic evolution of the model setup #A1: eclogite block size 25 km x 100 km, eclogite block density 3500 kg/m^3 , density differences 60 kg/m^3 .

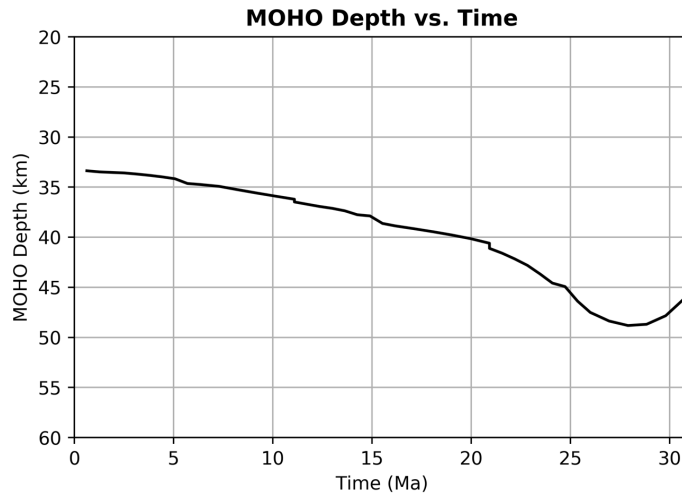


Figure 3.3 : MOHO vs. time (at $x=1000$ km).

As a result of this, mantle lithosphere begins to flow into the asthenosphere due to gravitational instability. The surface topography observed after 10 Ma shows a 500 m deep depression due to downward pulling of the eclogite. While MOHO depth increases laterally in parallel to the width of the eclogite block, and a small depression is observed on the middle with short wavelength undulations near the edges of eclogitic block. When $t=15$ Ma, topography begins to rise again in order to reach the isostatic equilibrium. After 20 Ma, the amount of material moving from mantle lithosphere to asthenosphere increases, because of the small-scale convective motion. At the last time period, the depth of the LAB varies from 175 km to 300 km and the elevation of the surface topography is fixed around 300 m. The depth of MOHO has measured to be 48 km on the deepest part (Figure 3.5).

3.1.1.3 Experiment #A3

In this model 5 km thick and 500 km wide eclogite body, with a density of 3500 kg/m^3 , has imposed into the setup. Mantle lithosphere is 200 km thick and has a density of 3330 kg/m^3 . Density difference between the mantle lithosphere and the asthenosphere is 60 kg/m^3 .

Since the eclogite has a density of 3500 kg/m^3 , it causes a gravitational instability between the mantle lithosphere and the asthenosphere (Figure 3.6). Therefore, small-scale convection cells that occur in asthenosphere causes sinking of the mantle lithosphere into the asthenosphere. Because of the dense eclogitic body, the downward movement begins to occur at $t=10.14$ Ma.

The short depressions observed in the surface topography that are equivalent to the width of eclogite block. About 20 Ma, the mantle lithosphere begins to break into pieces of the asthenosphere.

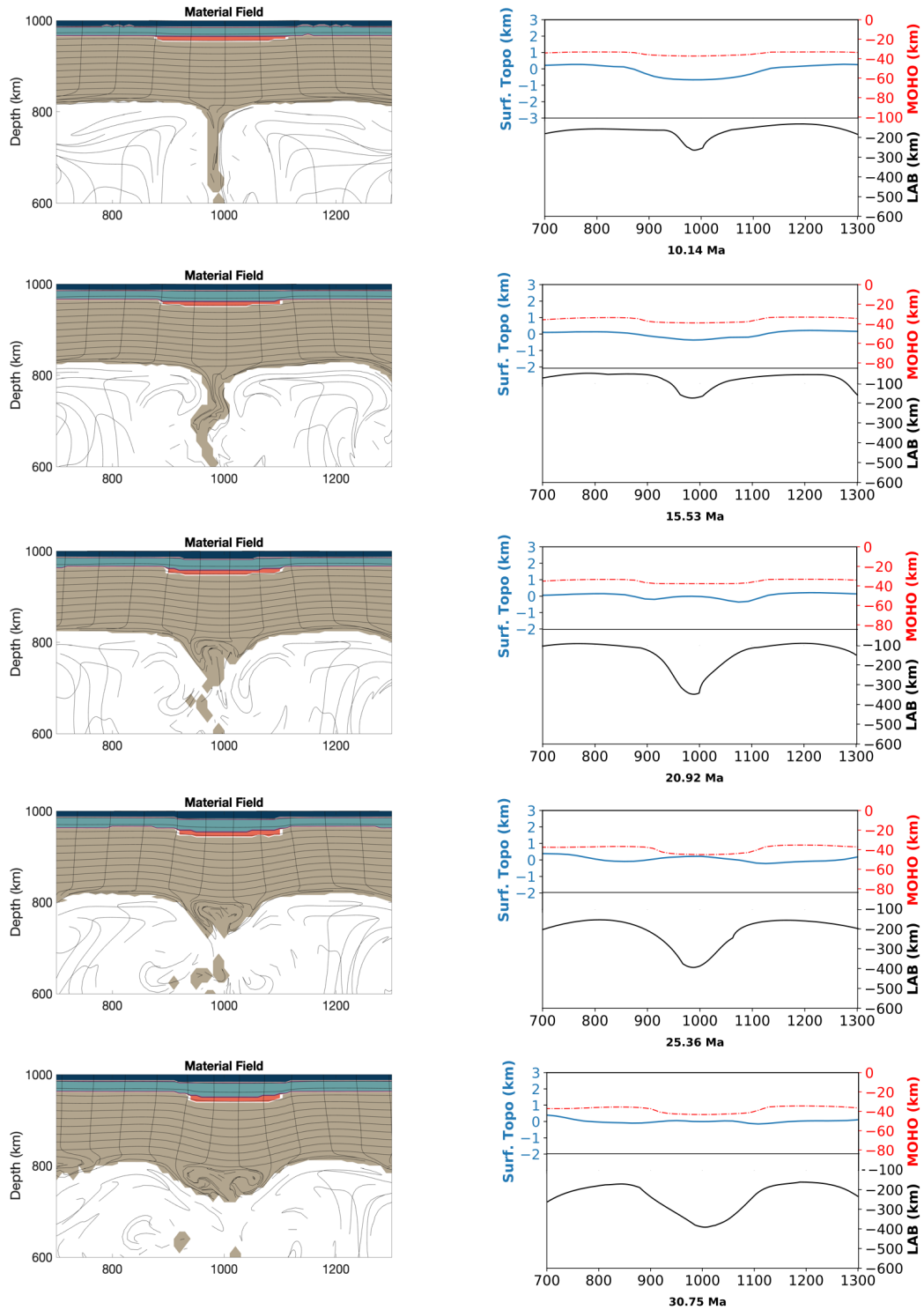


Figure 3.4 : Geodynamic evolution of the model setup #A2: eclogite block size 10 km x 250 km, eclogite block density 3600 kg/m³, density differences 40 kg/m³.

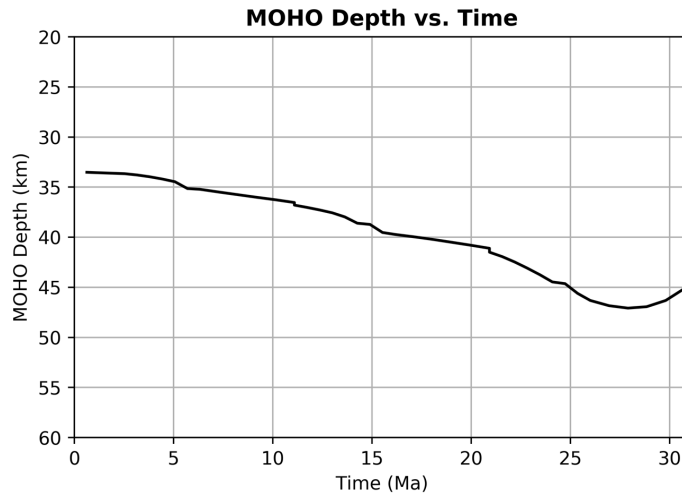


Figure 3.5 : MOHO depth vs. time (at $x=1000$ km).

At the end of 25 Ma, the MOHO depth begins to deepen due to pulling down in the ductile lower crust. In the last time period, convection movement in the asthenosphere initiates an increase in the surface topography, which leads to the drag of the accumulated area at the base of the mantle lithosphere. It was observed that the depth of MOHO decreased to approximately 38 km and the depth of LAB undulated between 315 km and 370 km (Figure 3.7).

3.1.2 Non-localized deformation

Experiments showing considerable removal of mantle lithosphere without an eclogitic drip has been classified as “non-localized deformation”. Experimental results indicate that, this behavior can be observed when density difference between the mantle lithosphere and the asthenosphere is 20 kg/m^3 or less ($\Delta\rho = 20 \text{ kg/m}^3$). Small-scale convection motions in the asthenosphere cause the instability of the mantle lithosphere along the LAB.

3.1.2.1 Experiment #B1

In this model 5 km thick and 500 km wide eclogite body, with a density of 3700 kg/m^3 , has imposed into the setup. Mantle lithosphere is 200 km thick and has a density of 3370 kg/m^3 . Density difference between the mantle lithosphere and the asthenosphere is 20 kg/m^3 .

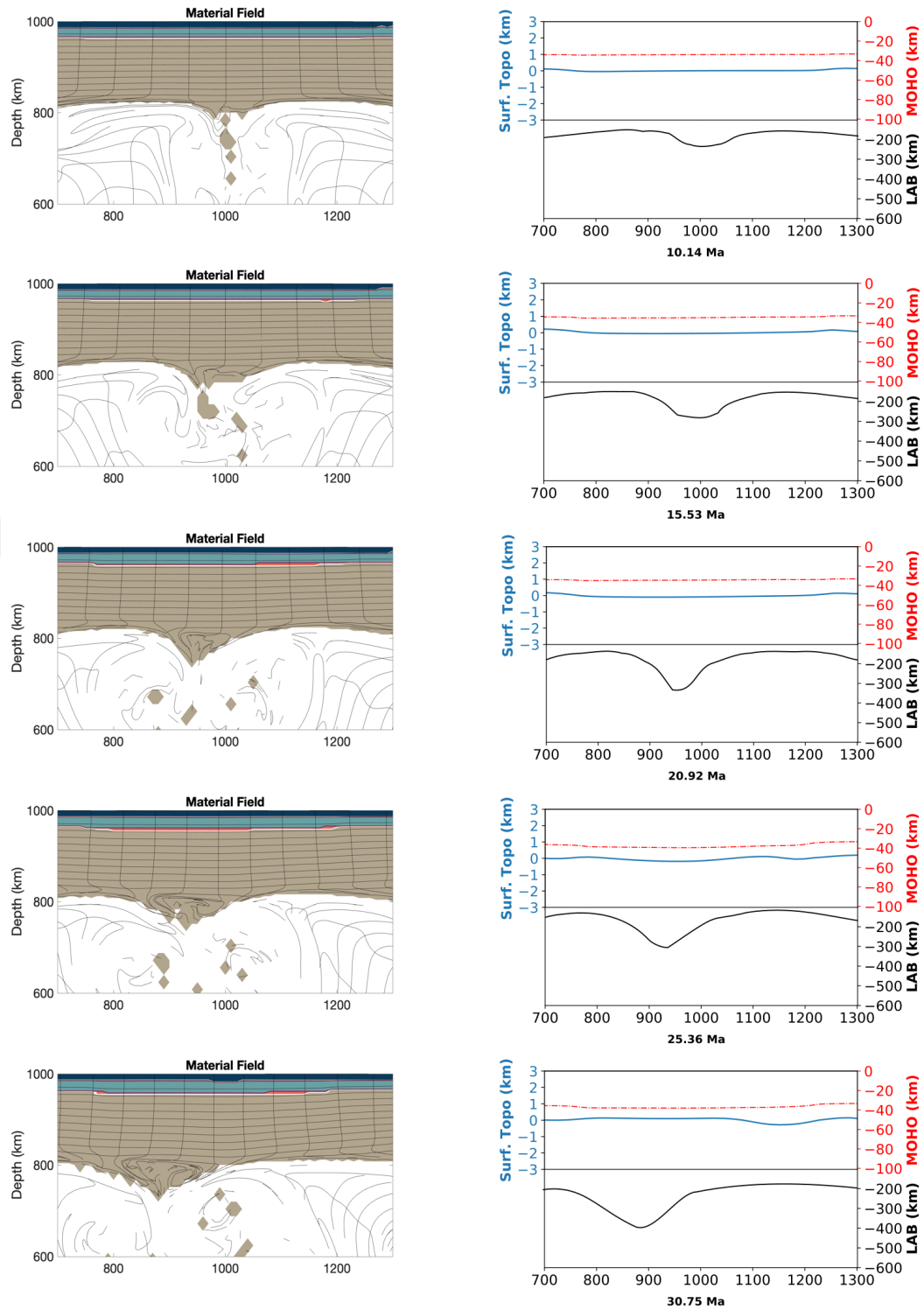


Figure 3.6 : Geodynamic evolution of the model setup #A3: eclogite block size 5 km x 500 km, eclogite block density 3500 kg/m³, density differences 60 kg/m³.

Even though the eclogite is denser, it is also thinner and wider. As a result, it does not create significant changes on topography and MOHO thickness at first, when compared with other models (Figure 3.8).

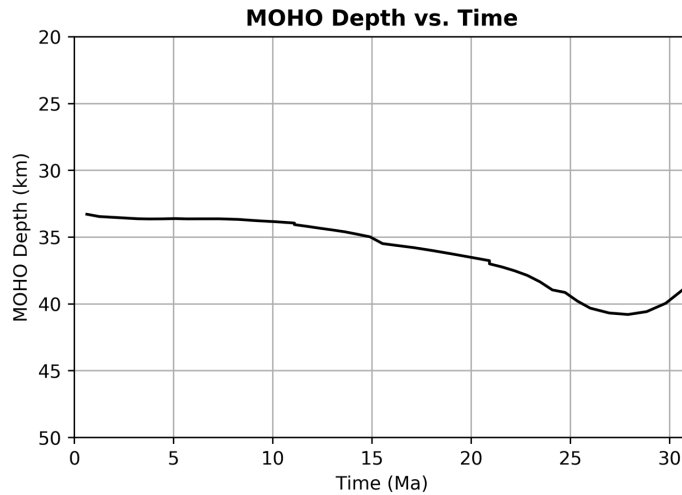


Figure 3.7 : MOHO vs. time (at x=1000).

When $t = 15.53$ Ma, negatively buoyant eclogite starts to pull down the lower crust on the middle sections of the model box, while MOHO depth decreases on the sides. Small scaled convection cells lead to removal of the lithospheric mantle on the sides. As the model evolves, middle sections of the crust and mantle lithosphere grow thicker while asthenosphere rises through the surface near the left and right boundary of the box. Eclogite thickens the overlying portions of the lower crust.

Thus, topography rises around 1km through the end of the model to reach to isostatic equilibrium. At the last time period, the thickness of MOHO reached down to a depth of ~ 57 km. It has been observed that MOHO depth increased from 35 km to 53 km in ~ 30 Ma (Figure 3.9).

3.1.2.2 Experiment #B2

In this model 5 km thick and 500 km wide eclogite body, with a density of 3600 kg/m^3 , has imposed into the setup. Mantle lithosphere is 200 km thick and has a density of 3370 kg/m^3 . Density difference between the mantle lithosphere and the asthenosphere is 20 kg/m^3 .

Thinner and wider eclogitic block does not create significant changes on topography and MOHO thickness at first, when compared with other models. When $t = 10.14$ Ma, negatively buoyant eclogite starts to pull down the lower crust on the middle sections of the model box, while MOHO depth decreases on the sides. Small scaled convection cells lead to removal of the lithospheric mantle on the sides (Figure 3.10). As the model

evolves, middle sections of the crust and mantle lithosphere grow thicker while asthenosphere rises through the surface near the left and right boundary of the box.

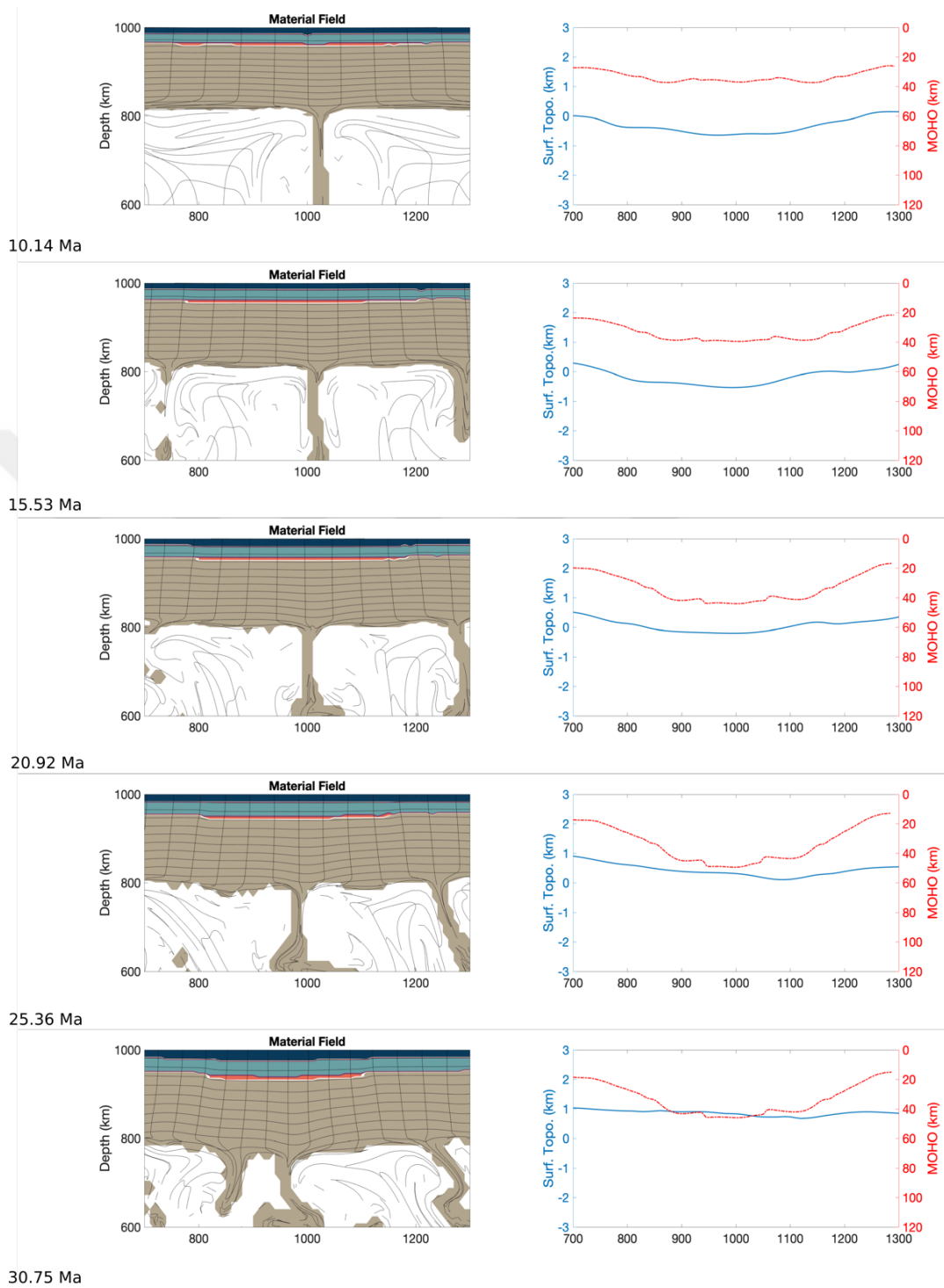


Figure 3.8 : Geodynamic evolution of the model setup #B1: eclogite block size 5 km x 500 km, eclogite block density 3700 kg/m³, density differences 20 kg/m³.

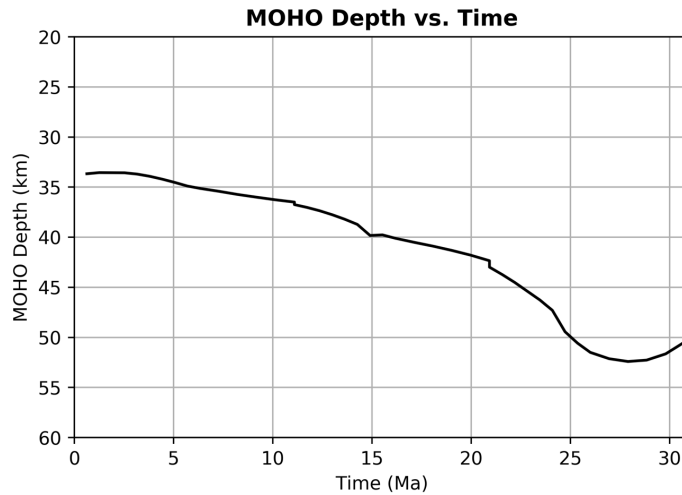


Figure 3.9 : MOHO vs. time (at $x=1000$ km).

Eclogite thickens the overlying portions of the lower crust. Thus, topography rises around 1km through the end of the model to reach to isostatic equilibrium. At the last time period, the thickness of MOHO reached down to a depth of ~ 57 km (Figure 3.11). It has been observed that MOHO depth increased linearly from 35 km to 53 km in ~ 30 Ma.

3.1.3 Pierce through

Deformation caused by the sinking eclogitic drip itself classified as “pierce through”. Separation of eclogitic body from the lower crust is the distinct feature of the models falling under this classification. Within time period used in the experiments, this behavior is only observed in some of the models with 25 km x 100 km eclogite size. Additionally, density of the eclogitic body must be sufficiently high enough to perform piercing through the mantle lithosphere (≥ 3600 kg/m³).

3.1.3.1 Experiment #C1

In this model 25 km thick and 100 km wide eclogite body with a density of 3600 kg/m³ has been used. Mantle lithosphere is 200 km thick and has a density of 3350 kg/m³. Density difference between the mantle lithosphere and the asthenosphere is 40 kg/m³. Thick and dense (negatively buoyant) eclogite starts to sink down and pulls the weak lower crust with it (Figure 3.12). Vertical displacement of the eclogite pushes down a portion of the mantle lithosphere into the asthenosphere.

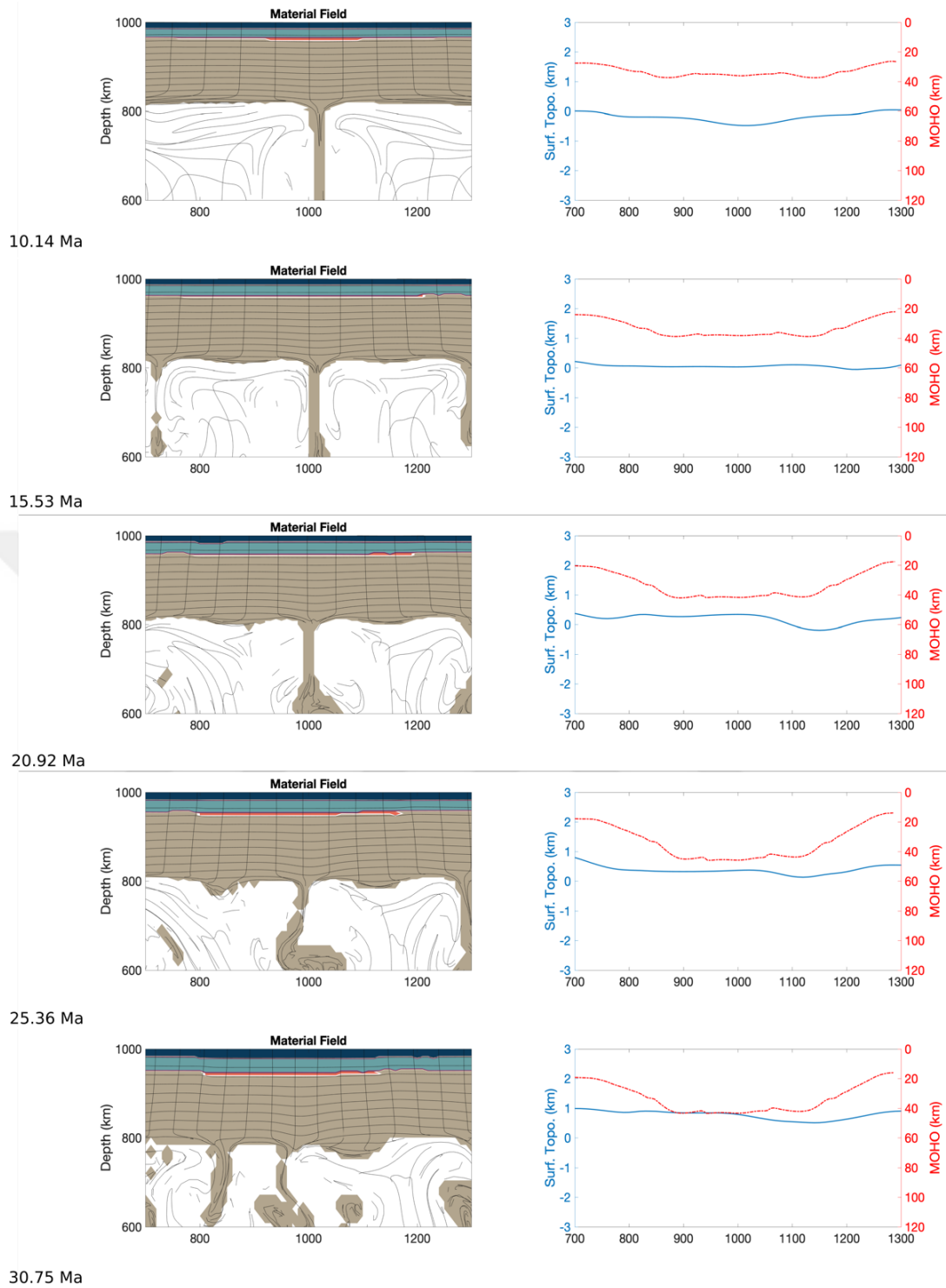


Figure 3.10 : Geodynamic evolution of the model setup #B2: eclogite block size 5 km x 500 km, eclogite block density 3600 kg/m³, density differences 20 kg/m³.

The downward movement of eclogite leads to thickening of the crust about 10-12 km in 10 Ma. The surface topography starts to rise after 10 Ma to provide isostatic balance.

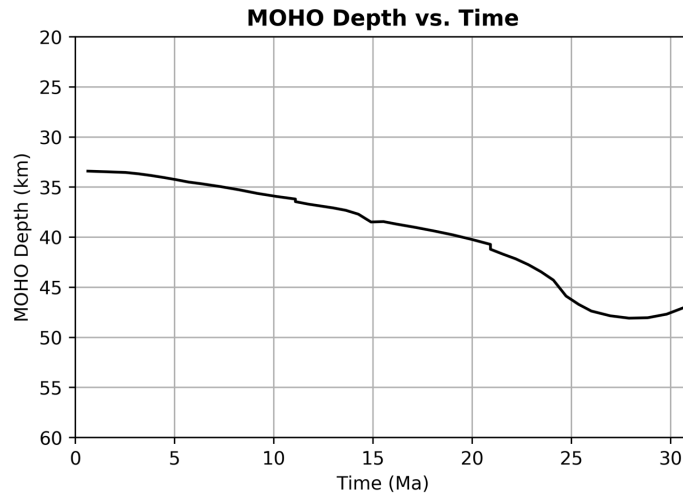


Figure 3.11 : MOHO vs. time (at x=1000 km).

After 15 Ma, the mantle lithosphere continues to sink from the middle of the box with the contribution of small-scale convection cells which have been formed on the both sides of the downwelling. After about 25 Ma, eclogite is almost separated from the lower crust.

In the last time period, eclogite descends into the asthenosphere with the mantle lithosphere. As a result of detachment of the eclogite from the lower crust, surface topography has risen to an elevation of 2.4 km. It has been observed that MOHO depth increased linearly from 42 km to 69 km in ~30 Ma (Figure 3.13).

3.1.3.2 Experiment #C2

In this model 25 km thick and 100 km wide eclogite body, with a density of 3600 kg/m³, has imposed into the setup. Mantle lithosphere is 200 km thick and has a density of 3330 kg/m³. Density difference between the mantle lithosphere and the asthenosphere is 60 kg/m³.

Although the density difference between the mantle lithosphere and the asthenosphere is 60 kg/m³, the eclogite block with a density of 3600 kg/m³ causes the system to become unstable (Figure 3.14). The downward movement of the eclogite block causes collapse in the surface topography as it pulls it down together with the lower crust. Due to thickening of the crust in 15Ma, the surface topography has increased parallel to width of the eclogitic body.

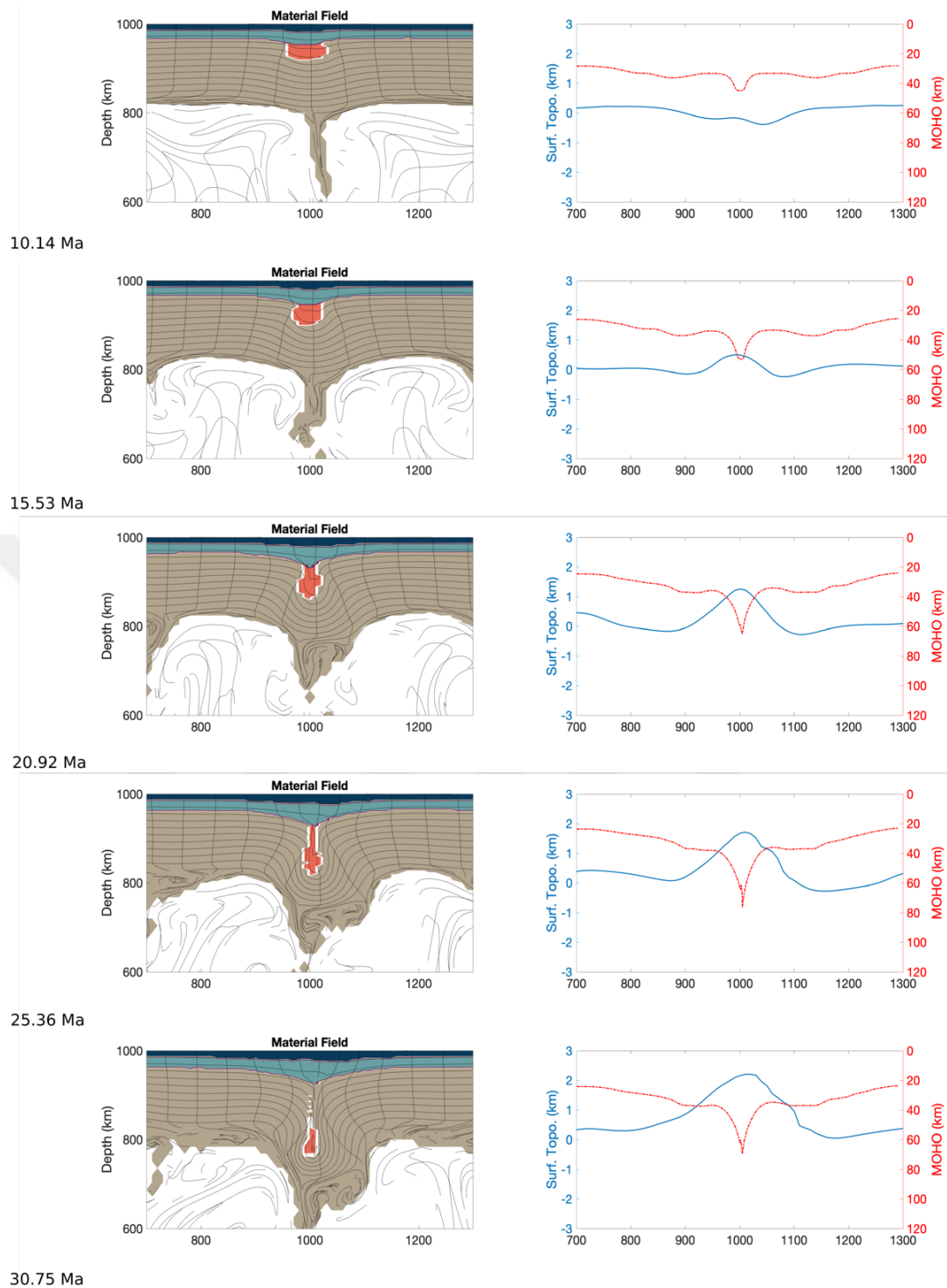


Figure 3.12 : Geodynamic evolution of the model setup #C1: eclogite block size 25 km x 100 km, eclogite block density 3600 kg/m³, density differences 40 kg/m³.

The mantle lithosphere is deformed by small-scale convection cells created by asthenosphere. About 25 Ma, the eclogitic block begins to break away from the lower crust. due to the pulling forces in the lower crust, the MOHO goes down to a depth of 70 km.

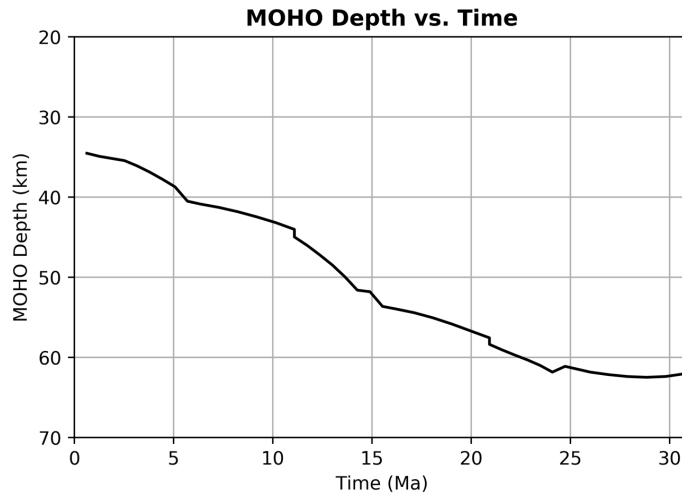


Figure 3.13 : MOHO vs time (at x=1000 km).

In the last time period, eclogite block breaks down from the lower crust and begins to drip into the mantle lithosphere. Due to increasing temperature, the dense block is disintegrated in the mantle lithosphere. Surface topography is approximately 2.5 km high, while the depth of MOHO reaches 70 km depth (Figure 3.15).

3.1.4 High degree deformation

In this deformation mode, the eclogite block becomes very unstable and creates several instabilities along the base of the mantle lithosphere, at first. Then, downward moving eclogite pushes a huge portion of the mantle lithosphere through the asthenosphere with itself. This process classified as “high degree deformation of the mantle lithosphere” because the initial geometry of these models has changed profoundly. The thickness of the eclogite block is the most important parameter leading to this deformation type. Decreasing thickness of the eclogitic block tends to result in “non-localized deformation” instead of high degree deformation. The decrease in density differences between the mantle lithosphere and asthenosphere is the secondary parameter controlling this deformation type (Figure 3.18). In some of the experiments with high degree deformation, the mantle lithosphere becomes completely removed in some parts, and crustal rocks becomes exposed to asthenosphere.

3.1.4.1 Experiment #D1

In this model 10 km thick and 250 km wide eclogite body, with a density of 3600 kg/m³, has imposed into the setup. Mantle lithosphere is 200 km thick and has a density

of 3390 kg/m^3 . Density difference between the mantle lithosphere and the asthenosphere is 0 kg/m^3 .

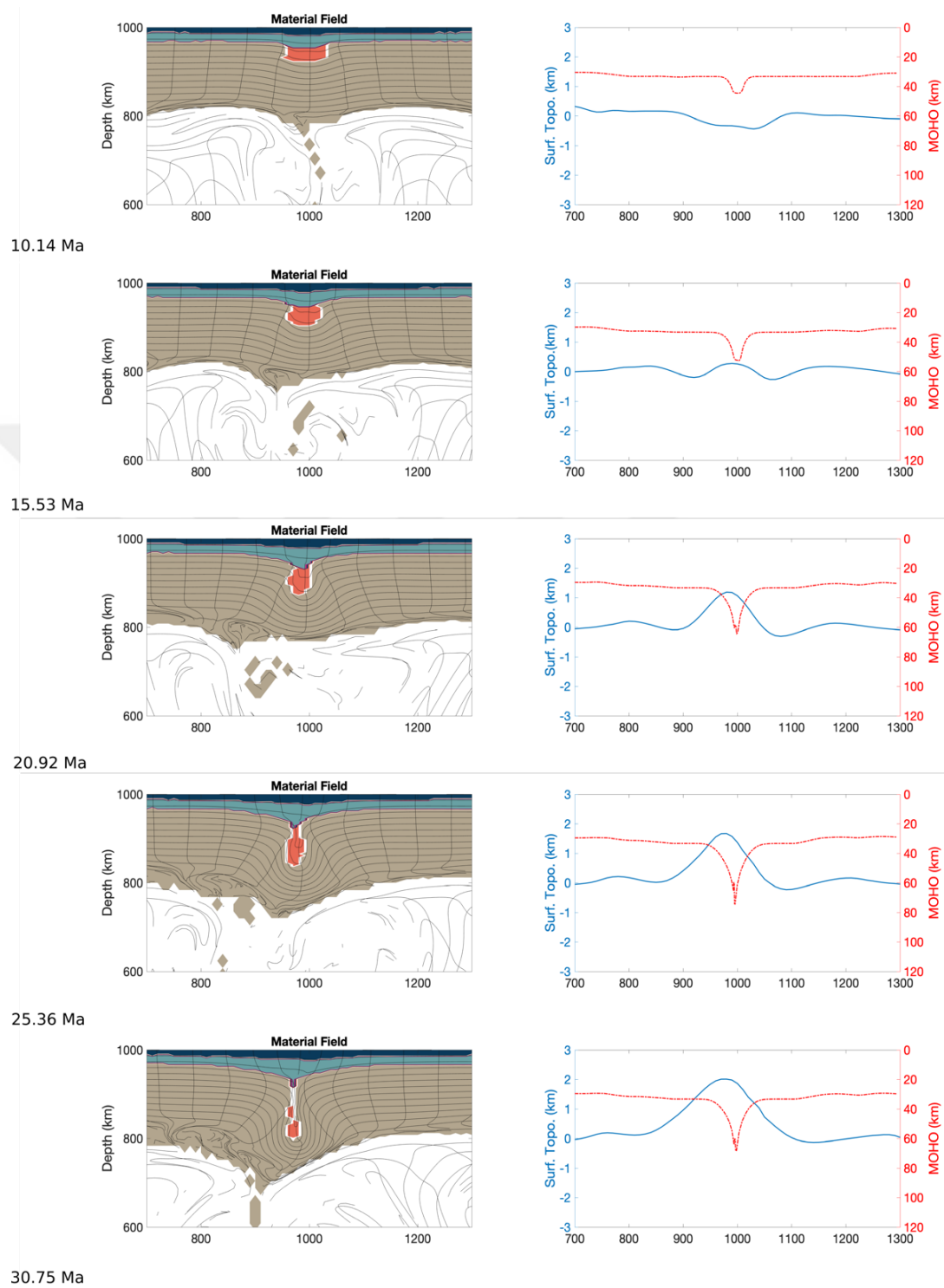


Figure 3.14 : Geodynamic evolution of the model setup #C2: eclogite block size $25 \text{ km} \times 100 \text{ km}$, eclogite block density 3600 kg/m^3 , density differences 60 kg/m^3 .

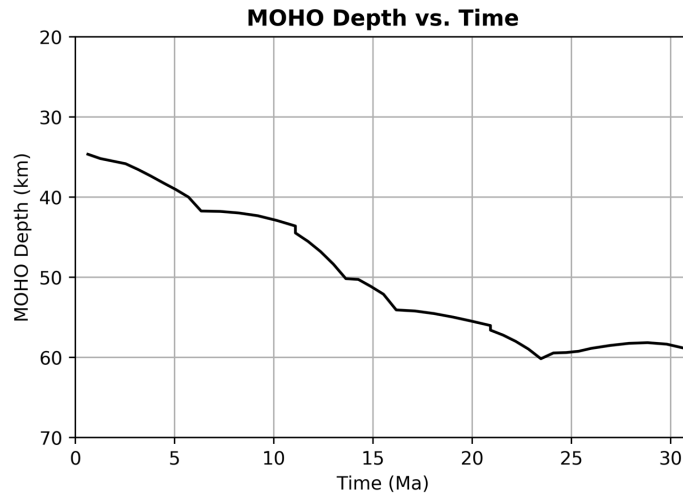


Figure 3.15 : MOHO vs. time (at x=1000 km).

The eclogite block causes the gravitational instability in the system. At the $x = 1000$ km, the mantle lithosphere begins to sink downwards (Figure 3.16). The convective movements taking place in the asthenosphere causes the mantle lithosphere to be deformed at the edges and gradually disintegrate. After 25 Ma, when the lower crust was pulled highly downwards by the eclogite, the surface topography showed an increase of 2 km and the depth of MOHO was approximately 90 km (Figure 3.17).

In the last time step, the eclogite block is detached from the lower crust and dripped into the asthenosphere within the mantle lithosphere. MOHO thickness decreases around 10 km as it is freed from the heavy block of eclogite, and surface topography elevated to 5 km.

3.2 Effect of Eclogite Size and Density

Model results indicate that, the thickness and width of eclogite have different effects on the system. The size and density of eclogite determines the behavior of the mechanism. Comparison of model results for varying eclogite and mantle lithosphere densities for different eclogite sizes shown in Figure 3.18.

- a) There is a limit between the eclogite densities where the eclogite does not detach from the lower crust and where it pierces through the lithosphere. Pierce through mechanism is only observed for the models with a 25 km x 100 km eclogitic block, when the eclogite density is 3600 kg/m^3 or 3700 kg/m^3 . If the mantle lithosphere density exceeds 3370 kg/m^3 , the system becomes unstable

and mantle lithosphere experiences a high-degree deformation. In some experiments, thickness of the mantle lithosphere becomes as thin as 50 km regionally, while some parts can be as thick as 350 km.

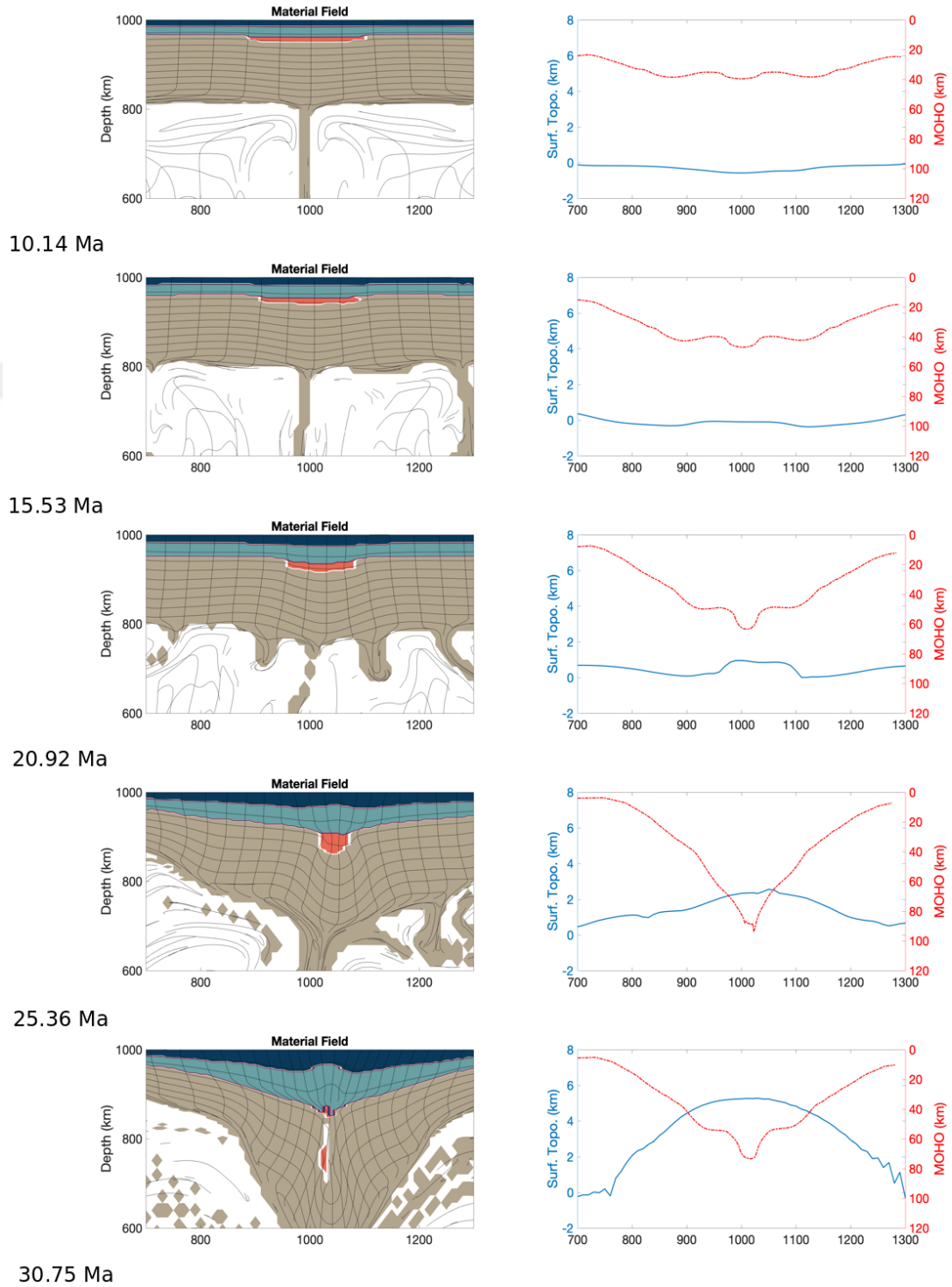


Figure 3.16 : Geodynamic evolution of the model setup #D1: eclogite block size 10 km x 250 km, eclogite block density 3600 kg/m³, density differences 0 kg/m³.

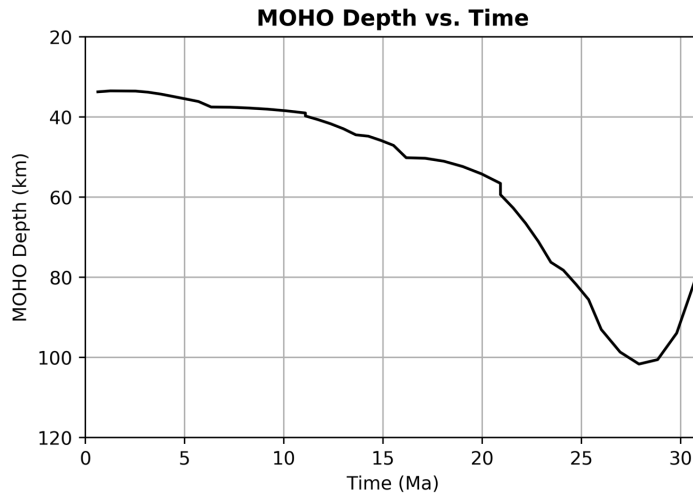


Figure 3.17 : MOHO vs. time (at $x=1000$ km).

- b) There are three mechanisms classified with the models that have $10 \text{ km} \times 250 \text{ km}$ eclogite size: (i) localized deformation, (ii) non-localized deformation and (iii) high-degree deformation of the mantle lithosphere (i.e. eclogitic blocks do not pierce through the lithosphere in any of these models, instead, eclogite remain within the mantle lithosphere). If mantle lithosphere density exceeds 3350 kg/m^3 in this model set, mantle lithosphere undergoes non-localized deformation until higher mantle lithosphere densities. When the eclogite densities were 3600 kg/m^3 and 3700 kg/m^3 , the major mechanism would be high degree deformation. In contrast, when mantle lithosphere density is equal to or lower than 3350 kg/m^3 , all of the models have been classified as “localized deformation”. Eclogitic drips was not observed in the experiments with a mantle lithosphere density is 3370 kg/m^3 or lower.
- c) Experiments carried out with $5 \text{ km} \times 500 \text{ km}$ eclogite give similar results to $10 \text{ km} \times 250 \text{ km}$ model set. Only difference between the two is, if mantle lithosphere is denser than 3350 kg/m^3 , eclogitic drip starts to sink but it remains trapped within the mantle lithosphere.

The width of eclogite leads to deformation of mantle lithosphere, while with increasing thickness eclogite pierces through the mantle lithosphere.



Eclogite Density vs. Mantle Lithosphere Density

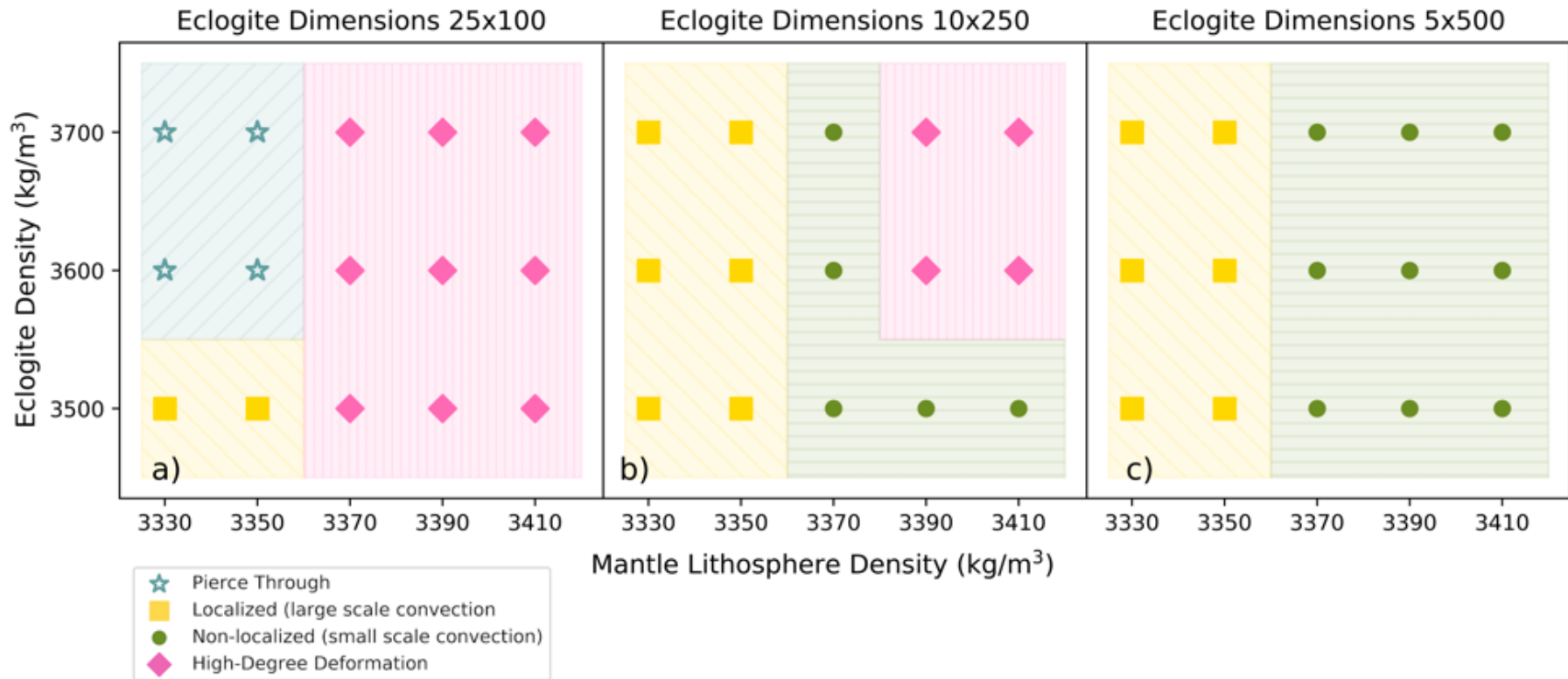


Figure 3.18 : Deformational behavior diagram.

3.3 Model Results Against Observations

The histograms of MOHO depth show the relation between mantle lithosphere and eclogite density (Figure 3.19, 3.20, 3.21). When model results grouped by the mantle lithosphere densities, all of the groups follow a linear trend with increasing eclogite densities. Mantle lithosphere density with 3390 kg/m^3 and 3410 kg/m^3 have not been chosen for comparison with observed data, due to unrealistic deformation in the mantle lithosphere.

Models classified as non-localized deformation, pierce through, and high degree deformation have not been chosen for comparison with observed data, due to unrealistic deformation in the mantle lithosphere. The minimum and maximum LAB depths for the different eclogite sizes are shown in Figure 3.22, 3.23 and 3.24. The histograms of LAB depth show the relation between mantle lithosphere and eclogite density. When model results grouped by the mantle lithosphere densities, none of the groups follow a linear trend with increasing eclogite densities.

The cross-sections taken from the MOHO and LAB depth maps prepared by Cherepanova & Artemieva (2015) are shown in Figure 3.25 (based on seismic velocity). The different cross-sections were taken from northwest – southeast (A-A'), west – east (B-B') and southwest – northeast (C-C' and D-D') directions. In the AA' cross-section taken from the MOHO map, increase of MOHO depth from 37 km to 49 km is observed from southeast through northwest. The MOHO depth for BB' section has an undulation pattern and thickness of MOHO varies between 41 to 48 km from west to east. In the section CC' taken from southwest to northeast an increase from 41 km to 48 km is observed. DD' cross-section have the deepest MOHO boundaries in the region which are ranging from 43 to 53 km. It was found that, MOHO depths obtained from some models were similar to certain parts of Siberian craton, at $5 \text{ km} \times 500 \text{ km}$ and $10 \text{ km} \times 250 \text{ km}$ eclogitic sizes. Pierce through and high-degree deformation models do not agree well with the MOHO thicknesses of Siberian Craton. It is observed that the depth of the LAB decreases abruptly from 180 km to 130 km in AA' cross section. There is a sudden increase in the depth of LAB from 180 km to 340 km for BB' cross-section.

The depth of LAB decreases from west to east (near eastern boundary of the craton) to 100 km depth. A more gradual increase is observed in CC' cross-section rather than a sudden increase in LAB depth.

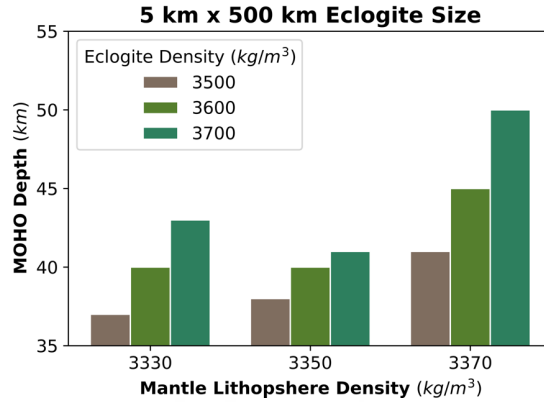


Figure 3.19 : Change in MOHO thicknesses with varying eclogite densities for 5 km x 500 km eclogite blocks.

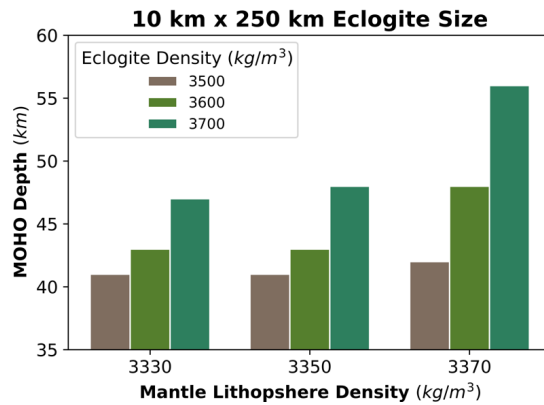


Figure 3.20 : Change in MOHO thicknesses with varying eclogite densities for 10 km x 250 km eclogite blocks.

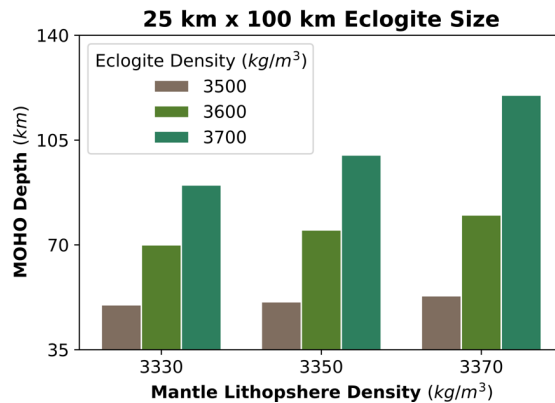


Figure 3.21 : Change in MOHO thicknesses with varying eclogite densities for 25 km x 100 km eclogite blocks.

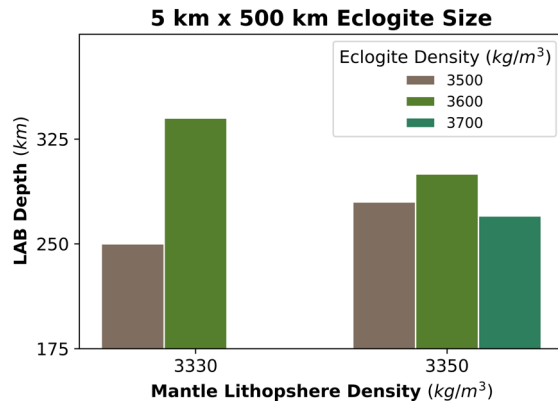


Figure 3.22 : Change in LAB thicknesses with varying eclogite densities for 5 km x 500 km eclogite blocks.

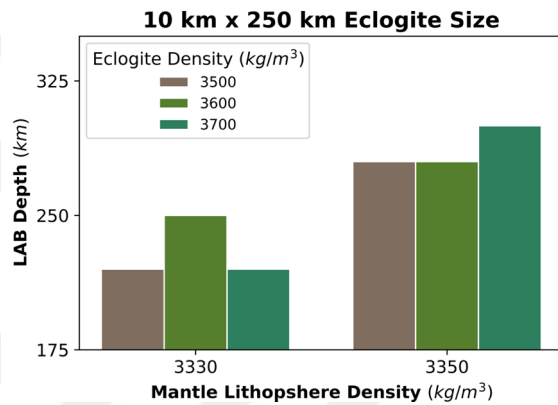


Figure 3.23 : Change in LAB thicknesses with varying eclogite densities for 10 km x 250 km eclogite blocks.

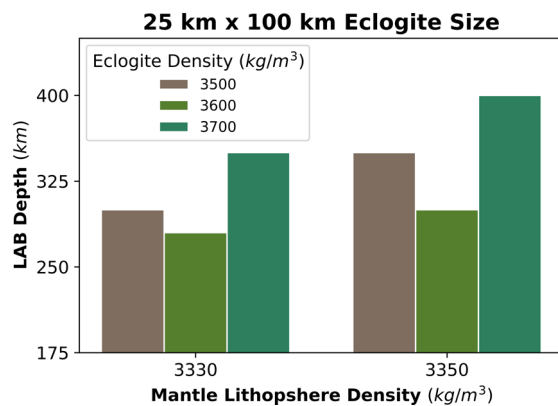


Figure 3.24 : Change in LAB thicknesses with varying eclogite densities for 25 km x 100 km eclogite blocks.

It is observed that the depth of LAB starting from approximately 200 km deepens to 350 km. An increase of 20 km in the depth of LAB is observed in the southwestern direction of the DD' cross-section (Figure 3.26).

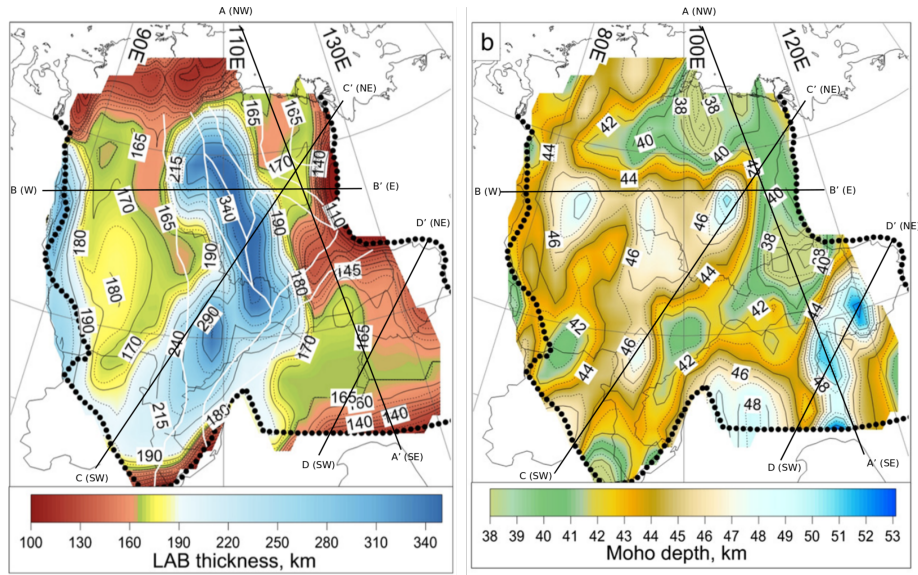


Figure 3.25 : MOHO and LAB depths (modified after Cherepanova & Artemieva, 2015).

Compared to other sections, the LAB depth does not differ significantly. The experiments reflecting localized deformation are in consistency with the observational data obtained from the depths of LAB provided by geophysical studies (Figure 3.27).

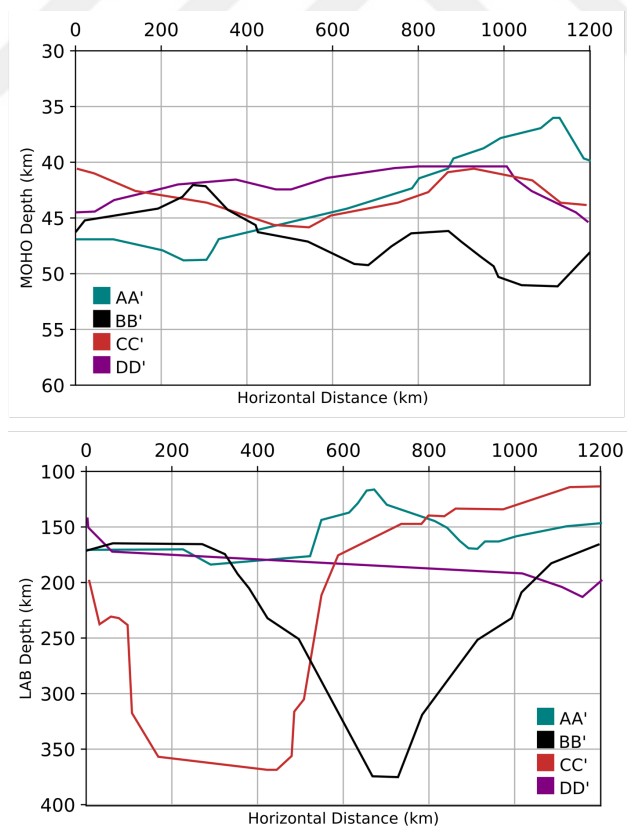


Figure 3.26 : MOHO and LAB depth vs. horizontal distance (cross sections taken from MOHO and LAB maps).

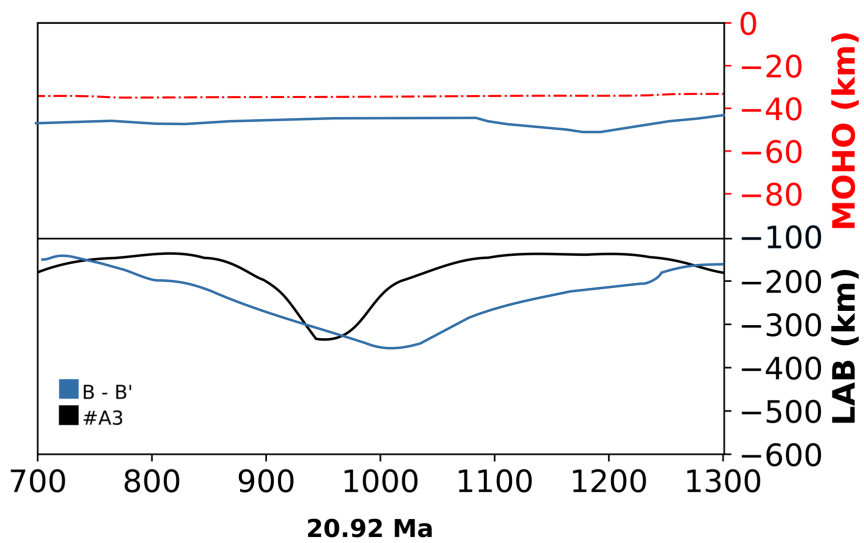
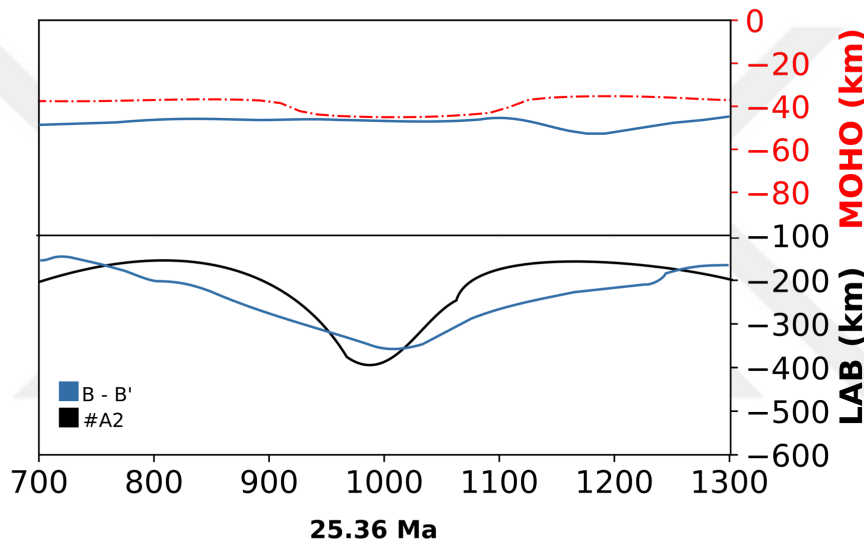
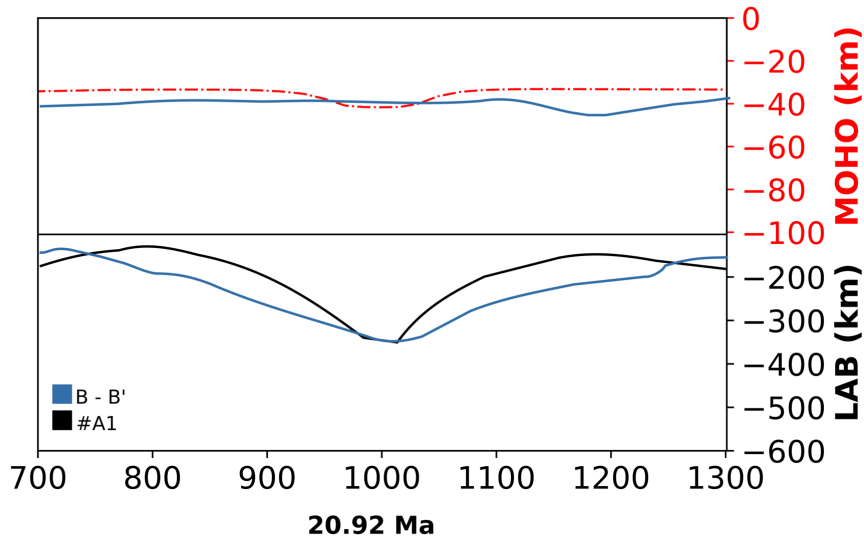


Figure 3.27 : MOHO and LAB depth comparison of real data with model results.

4. CONCLUSION

It has been found that the width and thickness of eclogite can display different results for MOHO and LAB thicknesses, and deformation behavior of the cratonic lithosphere. It has been observed that the models A1, A2 and A3 are consistent with MOHO and LAB thicknesses of BB' cross-section at $t = 20.92$ Ma, $t = 25.36$ Ma, and $t = 20.92$ Ma, respectively (Figure 3.26).

The gravitational instability caused by the increase of the thickness of eclogite, triggers the pierce through mechanism even in the lesser eclogite densities. Although the increase in the width of the eclogite still leads to gravitational instability, the deformation of the mantle lithosphere becomes the dominant mechanism. Model results indicate that, increasing thickness of eclogite causes eclogitic dripping with or without mantle lithosphere (pierce through, high-degree deformation) while increasing width leads to non-localized deformation of the mantle lithosphere.

From the classification based on the behavioral system, it is understood that the eclogite existing under the lower crust may lead to a form of deformation within the cratonic regions if certain conditions are met. Nevertheless, comparison of the experimental results with the field data suggest that, the most viable mechanism for the region is "localized deformation". Eclogite does not necessarily need to drip in order to create undulations in MOHO or LAB depths. An eclogitic body, located beneath the lower crustal rocks in Siberian Craton is capable of changing the crustal and mantle lithospheric thicknesses without piercing through or leading to high degree deformation of mantle lithosphere.



REFERENCES

- Anderson, D. L.** (2008). The eclogite engine: Chemical geodynamics as a Galileo thermometer. In *Special Paper 430: Plates, Plumes and Planetary Processes*. [https://doi.org/10.1130/2007.2430\(03\)](https://doi.org/10.1130/2007.2430(03)).
- Artemieva, I.** (2011). The lithosphere: An interdisciplinary approach. In *The Lithosphere: An Interdisciplinary Approach*. <https://doi.org/10.1017/CBO9780511975417>.
- Artemieva, I. M., Thybo, H., & Cherepanova, Y.** (2019). Isopycnicity of cratonic mantle restricted to kimberlite provinces. *Earth and Planetary Science Letters*. <https://doi.org/10.1016/j.epsl.2018.09.034>.
- Artemieva, Irina M., & Mooney, W. D.** (2004). Thermal thickness and evolution of Precambrian lithosphere: A global study. *Journal of Geophysical Research: Solid Earth*. <https://doi.org/10.1029/2000jb900439>.
- Cherepanova, Y., & Artemieva, I. M.** (2015). Density heterogeneity of the cratonic lithosphere: A case study of the Siberian Craton. *Gondwana Research*. <https://doi.org/10.1016/j.gr.2014.10.002>.
- Cherepanova, Yulia, Artemieva, I. M., Thybo, H., & Chemia, Z.** (2013). Crustal structure of the Siberian craton and the West Siberian basin: An appraisal of existing seismic data. *Tectonophysics*. <https://doi.org/10.1016/j.tecto.2013.05.004>.
- Fullsack, P.** (1995). An arbitrary Lagrangian-Eulerian formulation for creeping flows and its application in tectonic models. *Geophysical Journal International*. <https://doi.org/10.1111/j.1365-246X.1995.tb05908.x>.
- Gladkochub, D. P., Pisarevsky, S. A., Donskaya, T. V., Ernst, R. E., Wingate, M. T. D., Söderlund, U., ... Hanes, J. A.** (2010). Proterozoic mafic magmatism in Siberian craton: An overview and implications for paleocontinental reconstruction. *Precambrian Research*. <https://doi.org/10.1016/j.precamres.2010.02.023>.
- Gleason, G. C., & Tullis, J.** (1995). A flow law for dislocation creep of quartz aggregates determined with the molten salt cell. *Tectonophysics*. [https://doi.org/10.1016/0040-1951\(95\)00011-B](https://doi.org/10.1016/0040-1951(95)00011-B).
- Hacker, B. R.** (1996). Eclogite formation and the rheology, buoyancy, seismicity, and H₂O content of oceanic crust. In *Geophysical Monograph Series*. <https://doi.org/10.1029/GM096p0337>.
- Herzberg, C., & Rudnick, R.** (2012). Formation of cratonic lithosphere: An integrated thermal and petrological model. *Lithos*. <https://doi.org/10.1016/j.lithos.2012.01.010>.
- Hirth, G., and Kohlstedt, D.L.,** (1996), Water in the oceanic upper mantle:

Implications for rheology, melt extraction and the evolution of the lithosphere: *Earth and Planetary Science Letters*, v. 144, p. 93–108, doi: 10.1016/0012-821X(96)00154-9.

- Jin, Z. M., Zhang, J., Green, I. W., & Jin, S.** (2001). Eclogite rheology: Implication for subducted lithosphere. *Geology*. [https://doi.org/10.1130/0091-7613\(2001\)029<0667:ERIFSL>2.0.CO;2](https://doi.org/10.1130/0091-7613(2001)029<0667:ERIFSL>2.0.CO;2).
- Jordan, T. H.** (1978). Composition and development of the continental tectosphere. *Nature*. <https://doi.org/10.1038/274544a0>.
- Kelemen, P. B., Hart, S. R., & Bernstein, S.** (1998). Silica enrichment in the continental upper mantle via melt/rock reaction. *Earth and Planetary Science Letters*. [https://doi.org/10.1016/S0012-821X\(98\)00233-7](https://doi.org/10.1016/S0012-821X(98)00233-7).
- Kelly, R. K., Kelemen, P. B., & Jull, M.** (2003). Buoyancy of the continental upper mantle. *Geochemistry, Geophysics, Geosystems*. <https://doi.org/10.1029/2002GC000399>.
- Kopylova, M. G., Beausoleil, Y., Goncharov, A., Burgess, J., & Strand, P.** (2016). Spatial distribution of eclogite in the Slave cratonic mantle: The role of subduction. *Tectonophysics*. <https://doi.org/10.1016/j.tecto.2016.01.034>.
- Kuskov, O. L., Kronrod, V. A., Prokof'ev, A. A., & Pavlenkova, N. I.** (2014). Petrological-geophysical models of the internal structure of the lithospheric mantle of the Siberian Craton. *Petrology*. <https://doi.org/10.1134/s0869591114010056>.
- Lee, C.-T. A., Luffi, P., & Chin, E. J.** (2011). Building and Destroying Continental Mantle. *Annual Review of Earth and Planetary Sciences*. <https://doi.org/10.1146/annurev-earth-040610-133505>.
- Liao, J., Wang, Q., Gerya, T., & Ballmer, M. D.** (2017). Modeling Craton Destruction by Hydration-Induced Weakening of the Upper Mantle. *Journal of Geophysical Research: Solid Earth*. <https://doi.org/10.1002/2017JB014157>.
- Pysklywec, R. N., & Cruden, A. R.** (2004). Coupled crust-mantle dynamics and intraplate tectonics: Two-dimensional numerical and three-dimensional analogue modeling. *Geochemistry, Geophysics, Geosystems*. <https://doi.org/10.1029/2004GC000748>.
- Ranalli, G.** (2008). Rheology of the lithosphere in space and time. *Geological Society, London, Special Publications*. <https://doi.org/10.1144/gsl.sp.1997.121.01.02>.
- Rosen, O. M., Condie, K. C., Natapov, L. M., & Nozhkin, A. D.** (1994). Archean and early proterozoic evolution of the siberian craton: A preliminary assessment. *Developments in Precambrian Geology*. [https://doi.org/10.1016/S0166-2635\(08\)70228-7](https://doi.org/10.1016/S0166-2635(08)70228-7).
- Rosen, O. M., Condie, K. C., Natapov, L. M., & Nozhkin, A. D.** (2008). *Chapter 10 Archean and Early Proterozoic Evolution of the Siberian Craton: A Preliminary Assessment*. [https://doi.org/10.1016/s0166-2635\(08\)70228-7](https://doi.org/10.1016/s0166-2635(08)70228-7).

- Snyder, G. A., Taylor, L. A., Crozaz, G., Halliday, A. N., Beard, B. L., Sobolev, V. N., & Sobolev, N. V. (1997).** The origins of Yakutian eclogite xenoliths. *Journal of Petrology*. <https://doi.org/10.1093/petroj/38.1.85>.
- Zhu, R. X., Xu, Y. G., Zhu, G., Zhang, H. F., Xia, Q. K., & Zheng, T. Y. (2012).** Destruction of the North China Craton. *Science China Earth Sciences*. <https://doi.org/10.1007/s11430-012-4516-y>.





CURRICULUM VITAE



Name Surname : Açelya BALLI

Place and Date of Birth : Adana – Turkey / 02.01.1992

E-Mail : ballia@itu.edu.tr

EDUCATION :

- **B.Sc.** : 2017, Istanbul Technical University, Faculty of Mines, Mineral Processing Engineering
- **M.Sc.** : 2019, Istanbul Technical University, Eurasia Institute of Earth Sciences, Geodynamics Programme